NTNU

Norwegian University of
Science and Technology

Integrating Battery into MMC Submodule using Passive Filter and Control Technique

Sigurd Byrkjedal Wersland

Master of Energy and Environmental Engineering
Submission date: June 2017
Supervisor: Lars Einar Norum, IEL
Co-supervisor: Anirudh Budnar Acharya, IEL

Norwegian University of Science and Technology
Department of Electric Power Engineering

Summary

The growing need and importance of Battery Energy Storage Systems (BESS) in grid support applications as well as in the transportation sector, has brought attention to the adaption of the Modular Multilevel Converter (MMC) to be used in BESS. The MMC is already known for its high efficiency, high voltage capability and good harmonic performance, but the modular arrangement of the converter also allows the battery to be implemented in a distributed manner. Known as a split-battery topology or split-storage. Connecting individual battery units directly into the submodules of the MMC. Opening the possibility of high AC-side voltage without a transformer even with low battery voltage.

However, the current flowing through the submodules inherently consists of oscillating components on top of the DC-component. This thesis show that these are at fundamental and 2nd harmonic frequencies with amplitude of two and one times the DC-component respectively. It is assumed that this is unacceptable due its negative impact on battery performance and lifetime. In most literature this is solved by interfacing the batteries with the submodules using a DC-DC converter. But this thesis explores the possibility of mitigating these components using a control technique and an interface consisting of a filter based on passive components.

More elaborate, the proposed technique is two-legged. **1.** injecting a circulating current that cancels the 2nd harmonic power fluctuation in the arms and hence submodules. **2.** Employing a resonant filter to mitigate fundamental component together with a lowpass filter.

The performance and feasibility of this technique is analyzed theoretically and through simulations. Resonant branch of the filter is analyzed in simple lab experiment. And results indicate that the proposed solution works and could be attractive, especially in applications where high reliability is of concern.

Sammendrag

Det økende behovet for batteribaserte energilagringssystemer både for nettstøtte og i transportsektor med mer, har rettet oppmerksomhet på forskning og tilpasning av Modular Multilevel Converter (MMC) for bruk i slike batterisystemer. MMC er allereder kjent for å være en konverter med lave tap, høy spennings- og kraftoverføringsegenskaper og gir lav harmonisk forvrengning. Men den modulære strukturen av denne typen konverter åpner også muligheten for å fordele batterienheter utover hele konverterstrukturen. Dette er kjent som en delt-batteri strategi, hvor hver individuelle batterienhet er koblet direkte til submodulene i MMCen. Dette medfører at høy AC-spenning kan oppnås selv med lav batterispenning, uten bruk av transformatorer.

Problemet med denne løsningen er at det også er store AC-komponenter i strømmen gjennom submodulene. Denne hovedoppgaven viser at disse AC-komponentene består av fundamental og andre harmonisk frekvens, med amplituder på henholdsvis en og to ganger DC-komponenten. Det er videre antatt at slike strømmer er uakseptable mtp. batterienes reduserte ytelser og levetid. Tidligere forskning og litteratur har løst dette med å implementere DC-DC-konvertere mellom submodul og batteri. Men denne hovedoppgaven utforsker isteden muligheten for å dempe disse AC-komponenten ved bruk en kontrollteknikk og et passivt filter mellom submodul og batteri.

Mer nøyaktig består strategien av følgende: **1.** injisere en sirkulerende strøm som kansellerer den andre harmoniske komponenten. **2.** ved hjelp av et resonansfilter, dempe den fundamentale komponenten, sammen med et lavpassfilter for resterende frekvenser.

Virkningen og gjennomførbarheten til denne strategien er analysert teoretisk og gjennom simuleringer. Labforsøk er gjort på resonansfilteret. Resultatene indikerer at den presenterte løsningen fungerer og kan være attraktiv, spesielt i applikasjoner hvor høy pålitelighet er viktig.

Preface

A lot of hard work has gone into this last master year, but this has also rewarded me with a considerable amount of new knowledge and new skills. I have found most of the work I have done very interesting and I have enjoyed the freedom of freely choosing topics to work on, even though not everything ended up contributing to this thesis.

The thesis has been written in an explanatory way, with the objective of providing understanding to the reader. Focusing on intuitive and efficient explanations. Many basic topics that are not directly relevant for the specific topic of the thesis are either left out or only given short sections instead of reproducing text from the specialization project.

I would like to thank phd student Anirudh Budnar Acharya, which in practice has been my main supervisor throughout this master year. He has shown extraordinary commitment to my project, and helped me out whenever I have needed it. Both in intuitive explanations, guidance and giving me the opportunity to publish a IEEE paper. I would also like to thank my professor, Lars Norum, and Vladimir Klubicka at the service lab.

At last, I would also like to thank the Department of Electrical Power Engineering at NTNU for the financial support they are providing me to travel and present a paper written from this thesis.

Sigurd Byrkjedal Wersland

Trondheim, Norway 11. june 2017

Publication

An IEEE paper is under construction comprising the content of this thesis. The digest has been approved for the IEEE COMPEL 2017 conference 9-12 July at Standford Univeristy, USA, where the final paper will be published. I have received financial support from the Department of Electric Power Engineering to travel and present the paper.

S. B. Wersland, A. B. Acharya, L. Norum, ”Integrating Battery into Submodule using Passive Technique”, *Control and Modeling for Power Electronics (COMPEL)*, Stanford, USA, 2017.

Table of Contents

List of Tables

List of Figures

Abbreviations and Nomenclature

MMC	=	Modular Multilevel Converter
BESS	=	Battery Energy Storage System
ESS	=	Energy Storage System
CHB	=	Cascaded H-bridge
BMS	=	Battery Management System
SOC	=	State of Charge
OCV	=	Open circuit voltage (here battery)
PWM	=	Pulse Width Modulation
HVDC	=	High-Voltage Direct-Current
ESR	=	Equivalent Series Resistance
MOSFET	=	Metal-Oxide-Semiconductor Field-effect Transistor
IGBT	=	Insulated-Gate Bipolar Transistor
THD	=	Total Harmonic Distortion
PI	=	Proportional-Integral (controller)
VSC	=	Voltage Source Converter
N	=	Number of submodules in an arm
V_{dc}	=	High voltage DC-link voltage
v_g	=	Phase-voltage grid side
i_g	=	Phase-current grid side
i_c	=	Circulating current
v_{arm}	=	Arm voltage
P_{arm}	=	Arm power
φ	=	Angle between grid-voltage and grid-current
PF	=	Power Factor
C_r	=	Capacitance in resonant branch
L_r	=	Inductance in resonant branch
R_r	=	ESR in resonant branch
f_r	=	Resonant frequency
C_{sm}	=	Submodule capacitance / lowpass branch capacitance
R_{sm}	=	ESR of c_{sm}
L_f	=	Lowpass inductor (in series with battery)
R_f	=	ESR of L_f
R_{bat}	=	Battery internal resistance
v_{bat}	=	Battery open circuit voltage

Chapter 1

Introduction

This chapter will provide a context for the objective of this thesis. Introduce the fundamental operation and dynamics of the Modular Multilevel Converter (MMC). Provide basic understanding of Battery Energy Storage Systems (BESS). And address some of the challenges of realizing a MMC based BESS, which will be investigated further in the next chapters.

1.1 Modular Multilevel Converter

The MMC, also known as M2C or M^2C, was first proposed in [4]. And it refers to the converter structure consisting of the series connection of identical submodules forming what in the MMC is referred to as an arm. This structure is already known from the Cascaded H-Bridge (CHB) from [5]. But by series connecting two such arms in each phase-leg, the MMC also provides a high voltage DC-link. Making it especially attractive to use in HVDC-links, with its superior performance over conventional solutions available for high voltage and high power conversion. This has led to extensive research on this topology over recent years, also for many other applications. Such as Satic Var Compensation (STATCOM), electric drives, frequency converters and battery energy storage systems (BESS). Taking advantage of the MMCs highly scalable nature, controllable active and reactive power, low harmonic content and high efficiency.

Several submodule topologies exists ([6], [7]) and the branches can be configured for any number of phases and for DC-AC, AC-AC or DC-DC as well as star and delta configurations. But most literature is focused on the three-phase DC-AC configuration with halfbridge submodules shown in figure 1.1. This is the only configuration considered in this thesis.

1.1.1 MMC structure and operation

The halfbridge submodule illustrated in figure 1.1 can either insert or bypass the voltage of the submodule capacitor. If the same number of submodules are inserted inside one phase-leg at all times, the voltage will be constant over that leg. But the voltage at the midpoint AC terminal depend on the distribution of inserted submodules in upper and lower arm. Notice that adding the waveforms in figure 1.1(a) and 1.1(b) will give a constant value of 600 V. But subtracting them results in the waveform in 1.1(d), which is the phase voltage on the AC-side ($N + 1 = 5$ voltage levels). This makes the MMC able to produce a waveform with conceptually any number of voltage steps, only by adding more submodules in each arm. Unlike conventional converters, the switches found in the submodules of the MMC only need to block the submodule voltage, which is equal to the voltage steps on the AC-side. This way controllable switches (usually IGBTs) can be used even for high DC and AC voltages. And considering the potentially high number of voltage steps, good harmonic performance can be achieved even with low switching frequencies, which in turn can be utilized to reach very high efficiency.

On the downside the MMC topology requires a very high number of active components. Also, the complex structure of the MMC have some inherent internal dynamics which needs to be attenuated by the control system. Inevitably also making the control design more challenging.

1.1.2 Dynamics, modulation and control

Although many conventional control and modulation techniques can be applied to the MMC, there are also many specific features. Especially in the internal dynamics.

The arm currents are unlike conventional converters characterized by a continuous current flow. And instead of large DC-link capacitors, the storage elements are distributed throughout the submodules, giving the arms a capacitive nature. This arm current will charge and discharge the submodule capacitors, giving rise to the necessity of balancing their voltage [8].

Furthermore, without unrealistically large submodule capacitance and arm inductance, there will flow a circulating current inside the parallel connected phase-legs. Induced by the inevitable voltage fluctuation of the submodule capacitors. This current will not affect DC and AC side, but increase internal losses. Therefore this also needs to be attenuated by the internal control system. This current also opens a possibility to manipulate the arm currents, which will be exploited later in this thesis.

Modulation

Several modulation techniques exists. They can be divided into carrier-based and non-carrier-based. The carrier-based techniques can further be divided into Phase-shifted [9] and Level-shifted [10], [11]. Only depending on how the triangular wave is compared with the reference wave.

Non-carrier-based techniques include space-vector modulation [12], Nearest-Level mod-

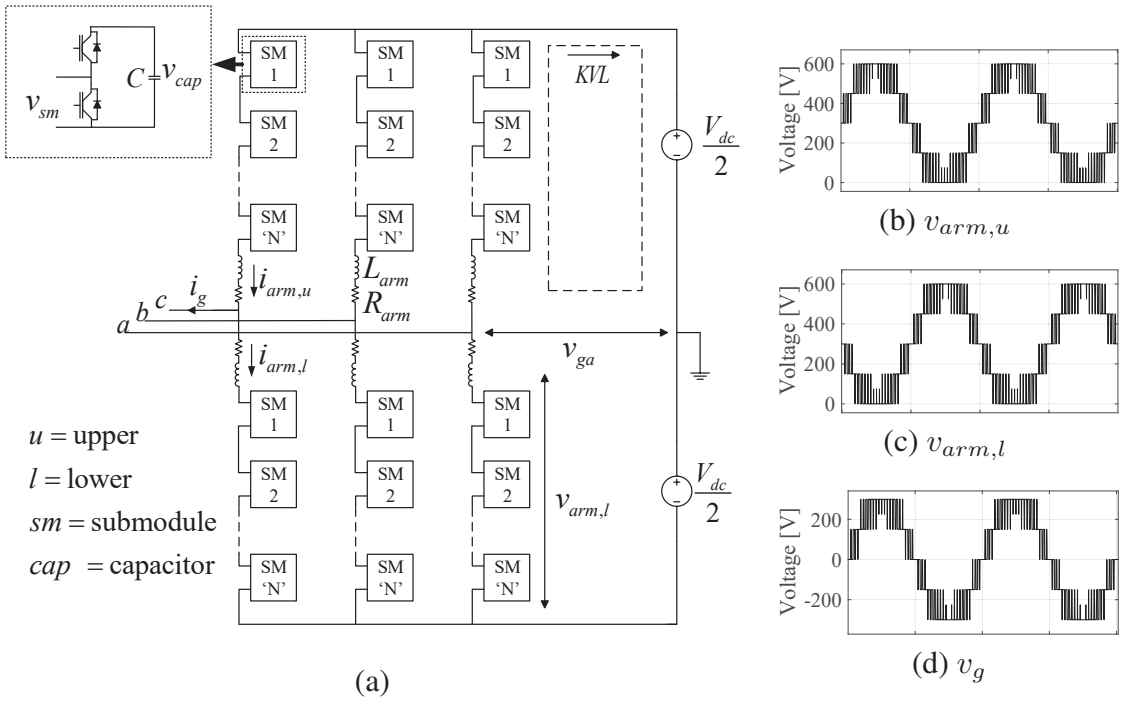

Figure 1.1: (a) MMC circuit overview, (b-d) illustrated arm voltages and grid phase-voltage for $N = 4$ MMC PS-PWM modulation

ulation [13] and Selective Harmonic Elimination [14] among others.

All these methods can also be further divided into $\big(N+1\big)$ techniques and $\big(2N+1\big)$ techniques, which referrers to the number of output voltage levels they will provide. N is the number of submodules in each arm. $\big(N+1\big)$ is the maximum number of levels achievable with a constant number of inserted submodules in each leg. The $\big(2N+1\big)$ techniques will cause this number to fluctuate with ± 1 which will cause the DC link voltage to fluctuate with the voltage of two levels. Which method is best suited, depends on configuration and application.

Dynamics

To develop the dynamical equations representing the MMC, KVL is used in one arm like illustrated in figure 1.1(a). By representing the voltage over the submodules or arm as:

$$v_{arm} = n_u v_{cu}^{\sum} \tag{1.1}$$

Where $v_{cu}^{\sum}$ is the sum of the voltages in all the submodules of the upper arm. n_u is the insertion indices, which represent the number of inserted submodules, where $n_u = 1$ means all the submodules in the arm is inserted and $n_u = 0$ means all the submodules in the arm is bypassed. This representation assumes that the submodule voltage is perfectly balanced.

KVL will then, for upper arm, give:

$$-\frac{V_{dc}}{2} + n_u v_{cu}^{\sum} + R_{arm} i_{arm,u} + L_{arm}\frac{di_{arm,u}}{dt} + v_g = 0 \tag{1.2}$$

And for lower arm:

$$-\frac{V_{dc}}{2} + n_l v_{cl}^{\sum} + R_{arm} i_{arm,l} + L_{arm}\frac{di_{arm,l}}{dt} + v_g = 0 \tag{1.3}$$

Using the arm currents $i_{arm,u}$ and $i_{arm,l}$ to define the ac current gives:

$$i_g = i_{arm,u} - i_{arm,l} \tag{1.4}$$

And the current flowing between the arms, not contributing to the AC current, known as the circulating current is defined as:

$$i_c = \frac{i_{arm,u} + i_{arm,l}}{2} \tag{1.5}$$

Substituting the arm currents in (1.2) and (1.3) with the definitions in (1.4) and (1.5) and subtracting upper arm from lower arm (1.2-1.3) give:

$$\frac{L_{arm}}{2}\frac{d}{dt}i_g = -\frac{R_{arm} i_g}{2} - v_g + \frac{(-n_u v_{cu}^{\sum} + n_l v_{cl}^{\sum})}{2} \tag{1.6}$$

Adding upper arm to lower arm (1.2+1.3) give:

$$L_{arm}\frac{d}{dt}i_c = -R_{arm} i_c + \frac{V_{dc}}{2} - \frac{(n_u v_{cu}^{\sum} + n_l v_{cl}^{\sum})}{2} \tag{1.7}$$

Together these two equations represents the average dynamical model of the MMC. (1.6) the outer grid dynamics and (1.7) the inner dynamics. This decoupling of the inner and outer dynamics, provides an important freedom in the control of the MMC.

Control

With (1.6) as basis, the outer grid controller can be designed. And very similar to conventional 2L-VSCs, transforming the dynamical equation to dq-frame using the Park-transformation, PI controllers can be used to control active and reactive power through the converter. Eventually modifying the last term in (1.6), the difference between insertion indices in upper and lower arm, which essentially is the reference signal for the converter.

Using (1.7) the circulating current can be controlled by an internal control loop. In regular DC-AC operation, this current is suppressed to avoid additional losses. Several techniques exists [15], all taking advantage of the dynamics in (1.7). The last term, the sum of insertion indices, is used to manipulate the reference signal without it affecting AC or DC side. This way the inherent 2nd harmonic component of the arm currents, i.e the circulating current, can be mitigated. The concept is essentially to slightly modify the reference signal so that it counteracts the inevitable voltage fluctuations of the capacitors. But this controller can also be utilized to *inject* a circulating current. And as for the ”self induced” circulating current, as long as it is injected in all three phase-legs and cancels each other, AC and DC side will remain unaffected. This particular feature of the MMC will be exploited later in this thesis.

1.2 Battery Energy Storage System

The increasing penetration of renewable energy resources (RES) in the power system is increasing the necessity of energy storage in the grid. RES tend to have an unpredictable and fluctuating nature such as solar and wind, which combined produced 8% of total electric power consumption in 2015 [16]. As fossil based energy resources are phased out, and such energy resources becomes the majority provider of electric power, large energy storage systems (ESS) will be needed to meet the daily, weekly and seasonal power demand fluctuations. In the transportation sector electric drives are replacing the internal combustion engine, and with it, the challenge of mobile ESS solutions arises.

As battery technology is evolving and cost is dropping, battery energy storage systems (BESS) will be an important part of the solution to these challenges.

1.2.1 Batteries and BMS

Battery systems are made up from battery cells, which are small energy units with low voltage and tolerate very limited operating conditions. Many different battery chemistry's exists and is used today depending on application. Lead-Acid, Nickel-Cadmium and Lithium-ion batteries are all common chemistry's. But Lithium-ion is today the superior chemistry on energy density, efficiency and as prices are dropping is becoming competitive even for stationary BESS. The drawback with Litium-ion is safety. If they are not operated within very tight limits they can be severely harmed or in worst case heat up to thermal runaway, where the cells burn up or explode. This sets strict requirements to the battery management system (BMS) that need to monitor, balance and operate the battery unit safely.

To increase the capacity of a battery unit, cells are paralleled. Paralleled cells will always be balanced and is easy to operate. But from an electrical point of view, high voltage is preferred to lower losses. In a battery unit, this means series connection of cells. But when cells are series connected, they are no longer automatically balanced. Small differences in capacity and leakage current will inevitably result in different state of charge (SOC) between each series connected level. Figure 1.2(b) illustrates this problem, and points out how unbalance decreases total available capacity.

As a consequence, the BMS needs to monitor each level of a series connection and be able to balance them. The cost of higher voltage is therefore higher complexity of the BMS. Which finally leads to a maximum achievable voltage on a battery unit.

1.2.2 MMC and BESS

Connecting batteries to the AC-grid or a drive, DC-AC conversion is obviously needed. And the advantages of the MMC definitely make it an attractive option to conventional converters. Also, the modularity of a battery unit can also take advantage of the modular arrangement of the MMC. The MMC allows the battery units to be connected in each submodule instead of the main DC-link as illustrated in figure 1.2(a). This arrangement decouples the battery unit voltage from the AC voltage. By adding more submodules, conceptually any AC-side voltage can be achieved even with a low battery voltage.

This strategy also has its challenges. The control system of the MMC needs to be

able to balance the battery units, taking over parts of the BMS tasks. And in the case of unbalance, operate with voltage differences between the battery units. Similar challenges are also found for regular DC-AC operation of the MMC, and the concept of the control methods used to cope with them is presented in the next chapter.

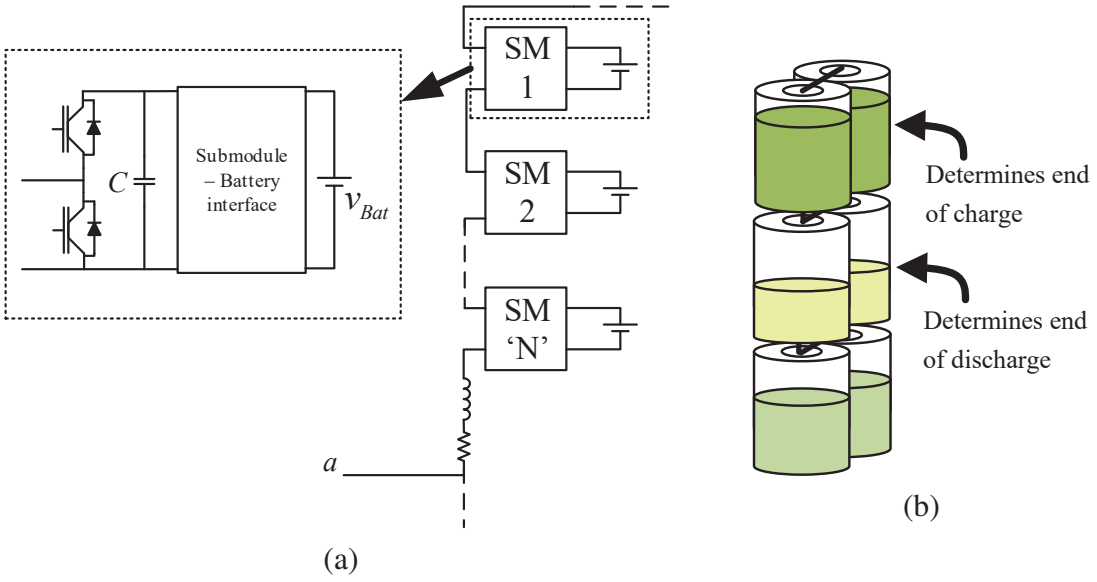

Figure 1.2: (a) MMC split-battery topology and (b) battery cells out of balance

1.2.3 Interfacing submodule and battery unit

Another important challenge is interfacing the batteries with the submodules. The submodules of the MMC ideally have constant voltage. This is what makes it possible to connect batteries to the them. But the current flowing through the arms and hence the submodules are AC-currents. After the submodules have chopped this current, there are still large AC-components present. It is not optimal for batteries to operate under such conditions. Therefore, different interfacing solutions have been suggested in literature to cope with this challenge. The main solution has been to use a DC-DC converter as interface [17], [18] and [19]. But also a direct interface only consisting of a filter using passive components have been proposed [1], although not researched to a large extent. The next chapter will give an overview of these solutions, and the rest of this thesis will investigate what will be referred to as the passive interface.

1.3 Motivation and problem description

This chapter has so far already presented the motivation of why BESS technology is important for the future and why the converter structure of the MMC can be suited also for such applications. And there already exists extensive literature on this topic, but there is little research on the alternatives to active DC-DC interfaces between battery and submodules in the MMC split-battery structure. And this is what will be explored in this thesis.

In general the objective is to analyze a strategy of using both a control technique and a passive interface to filter the inherent alternating current that otherwise would flow through the batteries in an MMC based BESS split-battery arrangement.

And more specifically, the objective is to analyze how a circulating current injection technique can lower the buffered arm energy fluctuations with the intention of lowering 2nd harmonic current flowing through the batteries. The second task is to design a passive filter with a resonant branch and a lowpass branch that can filter the remaining oscillating components. Mainly the fundamental component.

1.4 Thesis outline

Chapter 1 has given an introduction to fundamental operation of the MMC, basics on batteries and BMS, introduced how batteries can be integrated in an MMC and why these technologies are attractive and important for the future.

Chapter 2 will give a short review of the different interfacing strategies between battery units and submodules of the MMC. Next it will present the control concepts of battery balancing in an split-battery MMC topology. And how this is affected by using passive interfaces.

Chapter 3 will finally go deeper into the passive interface. First Analyzing the submodule currents that are to be filtered for the batteries. Then breaking the problem down to two parts. Attenuating the 2nd harmonic frequency component of the current using control strategy. And then designing a filter using passive components to attenuate the fundamental frequency. At last provide a simple analytic measure on the losses this strategy will introduce. All using a mathematical approach.

Chapter 4 presents the results from a Matlab/Simulink simulation model of an MMC with integrated batteries in the submodules. Providing results on how the passive filter and the control strategy performs in filtering the battery currents.

Chapter 5 presents results from a simple lab experiment on the resonant branch of the passive filter. And provides a discussion on challenges to realized this filter in the real world and especially the ratio between capacitance and inductance in the resonant branch.

Finally a **Conclusion** of the thesis is given, which also discusses future work that can be done on the topic.

Chapter 2

Modular Multilevel Converter with integrated BESS

2.1 Overview of Battery-Submodule interfaces

The focus of this thesis is on the passive interface. But to give an overview on the more researched alternatives, active interfaces are also presented in this chapter. [17], [18] and [19] all argues that this type of interface is the only feasible solution to prevent AC-components to flow through the battery.

2.1.1 Active interfaces

An active interface is essentially a bidirectional DC-DC converter that actively can control the voltage on the battery-side and submodule-side as well as the power flow between them. The advantage is therefor the degree of freedom for power flow control this interface provides. The battery current and voltage can easily be controlled in a safe manner, protecting the batteries. On the submodule-side, the voltage can also be controlled independent of the SOC of the battery. This leaves the MMC control to be a question about the dynamics between the DC-DC converter and the MMC itself. On the downside, this increases the hardware requirements and overall complexity of the system. The extra conversion stage will also introduce an additional source of losses to the system.

Non-isolated

Figure 2.1 show the schematic of of a non-isolated DC-DC converter. This is the topology discussed in [17], [18], [19] and is the active interface discussed in [1].

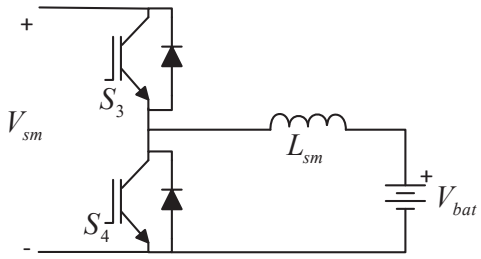

Figure 2.1: bidirectional halfbridge

It consists of a halfbridge, and an inductor in series with the battery. When S_3 is operated and S_4 is permanently blocking (working as a diode), the halfbridge functions like a buck-converter. Stepping down the voltage on the battery-side, with power flowing from submodule to battery (charging).

When S_4 is operated and S_3 is permanently blocking (diode), the halfbridge is working as a boost-converter. Stepping up the voltage for the submodule, with power flowing from the battery to the submodule (discharging).

Isolated

The flyback-converter is derived from the Buck-Boost converter and similarly as for the non-isolated case, using two switch-diode pairs, it can be modified to be a bidirectional converter.

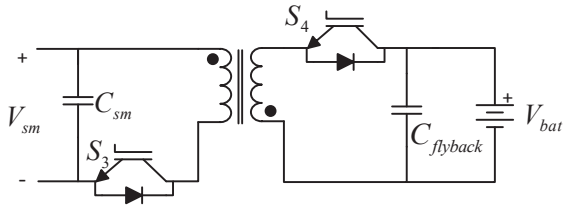

Figure 2.2: bidirectional flyback

When S_3 is operated and S_4 is blocking (diode), the power is flowing from submodule to battery (charging), operating as a regular flyback-converter, voltage depends on both the winding ratio of the high-frequency-transformer and the the duty ratio.

When S_4 is operated and S_3 is blocking (diode), power is flowing from battery (discharging) to submodule, again operating as a regular flyback.

The advantage of this isolation is that the batteries need no longer be on a floating potential and can be grounded. This could also open the possibility of paralleling all the battery units, into one large low voltage battery. Completely eliminating the challenge of SOC balancing between the distributed battery units.

2.1.2 Passive interface

The alternative to the active interface, is either no interface at all or some sort of passive interface. As already discussed, the passive interface is essentially a filter consisting of inductors, capacitors and resistors. The idea is that the filter can be designed so that it

filters out or mitigates the harmful AC-components to acceptable levels. Resulting in a solution with lower complexity and higher reliability then active interfaces.

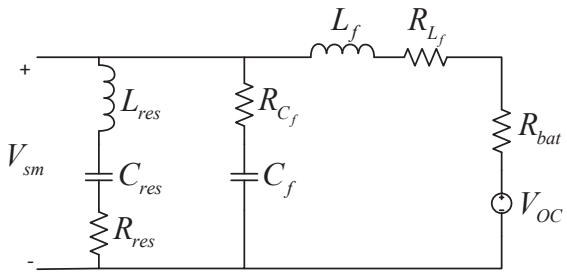

Figure 2.3: Passive interface from [1]

[1] proposed the passive interface shown in figure 2.3 to be used in a CHB submodule for battery integration. This is a combination of a lowpass filter and a resonant filter. The schematic includes all the parasitic equivalent series resistances, and the battery is modeled as a DC voltage source representing the open circuit voltage V_{OC} in series with the internal battery resistance R_{bat}.

L_{res}, C_{res} R_{res} makes up the resonant filter. C_f, R_{Cf}, L_f and R_{Lf} makes up the low-pass filter.

Simulation results in [1] indicated that such a solution could be feasible in the case of the CHB, where there are only one low frequency AC-component; the 2nd harmonic. The resonant filter can effectively remove this component without need for large passive components. Adding the lowpass filter only to filter the higher order switching harmonics.

The case is similar for MMC, but with one serious impediment; there are two low frequency components that needs to be filtered out. Both fundamental and 2nd harmonic. And this is essentially the topic of this thesis. How can the passive interface solution be adapted to the MMC, and is this feasible? This is investigated further from chapter 3.

2.2 Battery balancing

The concept of battery balancing and BMS was introduced in chapter 1. All battery units, especially Li-ion batteries that are series connected, need a fairly sophisticated BMS to be operated properly. In an MMC split-battery structure each battery unit placed in the submodules will need its own individual BMS. Assuming the units has series connected batteries. This will just have to be a conventional BMS, which is provided from many battery manufacturers. This will ensure that the battery cells within each battery unit is balanced with each other and is operated safely. But in the MMC split-battery structure there are many battery units, and it is crucial for the system as a whole that all these units are balanced with each other as well. And this is where merging BMS with the MMC control is needed. Creating a second or higher level of the BMS.

There are three alternative strategies to balance batteries. The first and most used in conventional BMSs on cell level is to ”burn off” energy in the cells with the highest SOC through some ohmic resistance. Balancing the cells at the SOC level corresponding to the cell with lowest SOC. The second strategy is to move energy between cells or battery units, balancing at the average SOC level (minus the losses in the process). The third and last strategy is to charge/discharge the cells or units at different rates dependent on their SOC. Which also will balance the batteries at an SOC level equivalent to the average level.

Although these last two strategies seems to be the most energy efficient, the complexity in the system needed to implement them on a cell level is often not feasible or introduce considerable losses. But in an MMC split-battery BESS this structure is already there. And the internal freedom of the MMC provides possibility to control the absorbed or injected power across the three ”axes” of the converter; between the submodules within an arm, between upper and lower arm and between the three phase-legs of the converter. The next three sections will explain the concept of these control objectives. Which are needed in regular MMC operation as well, to ensure equal charge of the capacitors through out the converter. But in the case of battery balancing, needs to handle a larger amount of energy transfer.

2.2.1 Submodule power control

Individual submodule power control refers to the ability of injecting or absorbing different amounts of power in the submodules inside the same arm. This way enabling balancing between the battery units within that arm. A very similar concept as is used to balance the capacitor voltage in a regular MMC can be employed to do this. Inserting the submodules with higher or lower SOC more often, depending on which direction the power is flowing. Which is done by adapting the respective modulation reference for each submodule with a power ratio factor β_{sm} according to [19]:

$$\beta_{sm} = \frac{\text{submodule active power}}{\text{arm active power}} \tag{2.1}$$

Or more accurately:

$$\beta_{kji} = \frac{\overline{v}_{sm}^{kji}\overline{i}_{sm}^{kji}}{\sum_{i=1}^{N}\overline{v}_{sm}^{kji}\overline{i}_{sm}^{kji}} = \frac{P_{sm}^{kji}}{\sum_{i=1}^{N}P_{sm}^{kji}} \qquad \text{where} \qquad \sum_{i=1}^{N}\beta_{kji} = 1 \tag{2.2}$$

$$\text{and} \qquad k, j, i = \text{phase, arm, submodule}$$

By multiplying the PWM controlled arm voltage with each respective power ratio factor, the total arm power can be distributed in the submodules in a desired manner.

2.2.2 Arm power control

Controlling the power of an arm or rather the difference in power between the two arms in a leg is where the benefit of the inherent circulating current in the MMC comes into play. And by analyzing the arm power equation this will become apparent. In regular MMC operation, where power is flowing between the high voltage DC-link and the AC-side, the arm power is on average zero (ideally). It will only fluctuate with the power buffered in the capacitors of the submodules. A DC-component in the arm power will charge or discharge the capacitors to a different voltage level. Which in a regular MMC is only used at start-up or shut-down, to charge or discharge the capacitors to the desired voltage level.

In MMC split-battery operation the arm power will have a DC-component corresponding to the power delivered or absorbed by the batteries. This makes sense since the batteries

or power sources are actually inside the arms. So first, lets derive the arm power equations. These will be useful to understand arm power control, and will be very central in chapter 3.

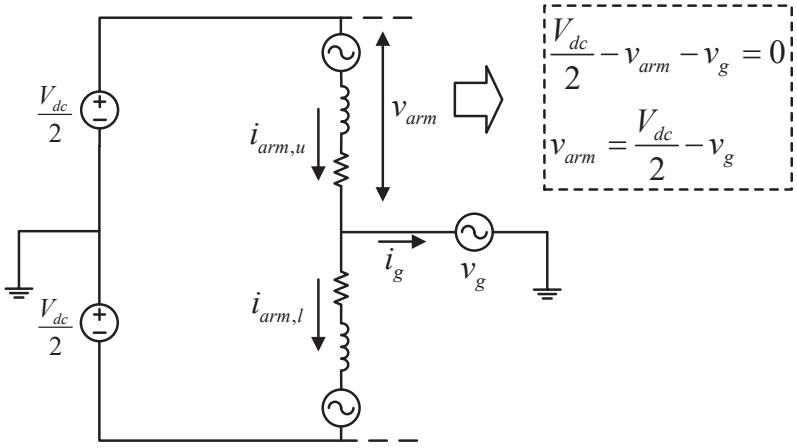

Figure 2.4: One arbitrary arm in the MMC. Deriving v_{arm}

The instantaneous arm power is the product of the voltage over the arm and the current flowing through it, $P = VI$, according to figure 2.4 this can be written as:

$$P_{arm,u} = (\frac{V_{dc}}{2} - v_g)i_{arm,u} \tag{2.3}$$

And similar for lower arm:

$$P_{arm,l} = (\frac{V_{dc}}{2} + v_g)i_{arm,l} \tag{2.4}$$

The arm current consists of two terms. Consistent with the definitions given in (1.4) and (1.5) and assuming the grid current splits perfectly into upper and lower arm, which it does in a balanced MMC. The upper and lower arm current can be defined respectively as:

$$i_{arm,u} = \frac{i_g}{2} + i_c \tag{2.5}$$

$$i_{arm,l} = -\frac{i_g}{2} + i_c \tag{2.6}$$

Giving the following expression for upper and lower arm power:

$$P_{arm} = (\frac{V_{dc}}{2} \mp v_g)(\pm\frac{i_g}{2} + i_c) \tag{2.7}$$

$$P_{arm,u} = \frac{V_{dc}}{2}\frac{i_g}{2} + \frac{V_{dc}}{2}i_c - v_g\frac{i_g}{2} - v_g i_c \tag{2.8}$$

$$P_{arm,l} = -\frac{V_{dc}}{2}\frac{i_g}{2} + \frac{V_{dc}}{2}i_c - v_g\frac{i_g}{2} + v_g i_c \tag{2.9}$$

At this point it is very useful to present the trigonometric identity in (2.10), relating the *product* of oscillating components with a *sum* of oscillating components:

$$\cos(\omega_a t)\cos(\omega_b t+\varphi)=\frac{1}{2}\Big[\cos\big(\omega_a t-(\omega_b t+\varphi)\big)+\cos(\omega_a t+\omega_b t+\varphi)\Big] \quad (2.10)$$

2.10 shows that:

$$50Hz*50Hz=150Hz+50Hz \quad (2.11)$$

$$50Hz*50Hz=100Hz+DC \quad (2.12)$$

Looking at (2.8) and (2.9) it is seen that the third term, $v_g\frac{i_g}{2}$, always will result in a DC-component. In regular MMC operation, the circulating current i_c will consist of a DC-component equal to $\frac{i_{DC}}{3}$ and, if not suppressed, a 2nd harmonic component. This will in turn produce another DC-component in the second term, $\frac{V_{dc}}{2}i_c$, which cancels the first DC-component. All the other components average to zero.

In a split-battery MMC structure, the circulating current has no DC-component since there are no current flowing from the high voltage DC-link. Instead the power is generated or absorbed from within the arms. Thus, using (2.10) on $v_g\frac{i_g}{2}$ will give the average arm power or active power delivered or absorbed by the batteries (assuming $\varphi=0$):

$$\begin{aligned}P_{arm,avg}&=\hat{v}_g\hat{i}_g\frac{1}{4}\Big[\cancel{\cos(2\omega t)}+1\Big]\\&=\sqrt{2}v_{g,rms}\sqrt{2}i_{g,rms}\frac{1}{4}\\&=\frac{1}{2}v_{g,rms}i_{g,rms}\end{aligned} \quad (2.13)$$

This makes sense since the total power at the AC-side will be $3v_{rms}i_{rms}$ and there are 6 arms in a 3-ph MMC.

So this is the power delivered or absorbed by each leg. They are equal in normal operation, but now it is also apparent how to introduce a difference between the upper and lower arm. Going back to (2.8) and (2.9), notice that the last term, $v_g i_c$, is added to upper arm and subtracted from lower arm. And remember that the circulating current can be controlled and take on whatever frequency, since it is only floating within the legs of the MMC. So if a circulating current at the fundamental frequency is impressed in the converter, (2.12) shows that it will result in a extra DC-component in the arm power equation. Added to upper arms and subtracted from lower arms.

$$\overline{v_g i_c}=\hat{v}_g\hat{i}_c\frac{1}{2}\Big[\cancel{\cos(2\omega t)}+1\Big]=\frac{1}{2}\hat{v}_g\hat{i}_c$$

Giving power for the upper arm:

$$\overline{P}_{arm,u}=\frac{1}{4}\hat{v}_g\hat{i}_g+\frac{1}{2}\hat{v}_g\hat{i}_c \quad (2.14)$$

And power for the lower arm:

$$\overline{P}_{arm,l} = \frac{1}{4}\hat{v}_g\hat{i}_g - \frac{1}{2}\hat{v}_g\hat{i}_c \tag{2.15}$$

So an injected circulating current at the fundamental frequency and in phase with v_g will have the following relationship between its amplitude and the arm power difference ΔP:

$$\Delta P_{arm} = P_{arm,u} - P_{arm,l} = \frac{1}{2}\hat{v}_g\hat{i}_c - \Big(-\frac{1}{2}\hat{v}_g\hat{i}_c\Big) \tag{2.16}$$

$$\hat{i}_c^{fnd} = \frac{\Delta P_{arm}}{\hat{v}_g} \tag{2.17}$$

But there is one more challenge; if the AC-side and DC-side of the converter is not to be affected, it implies that the sum of the circulating currents in each leg cancels each other. Ensuring that the circulating current stays inside the converter legs. But if different balancing powers are needed within each of the three phase-legs, this will imply different circulating current injections in each leg. According to [2] power exchange in one phase is decoupled from the other two phases if circulating currents with half the amplitude and 90 degrees phase shift from their respective phase voltages is injected in the other two phases. This will ensure that only reactive power is exchanged in these two phases and provides full circulating current cancellation. This is illustrated in figure 2.5. Finally enabling energy balancing between upper and lower arm inside each individual leg.

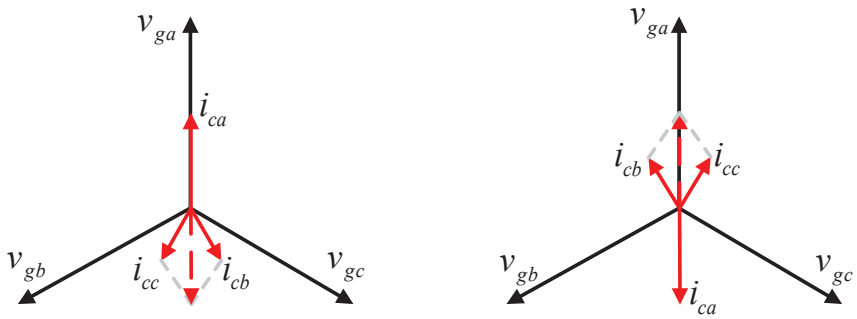

Figure 2.5: Angle of 2nd harmonic circulating current component for each phase in relation to phase voltages. Similar to figure in [2]

2.2.3 Phase-leg power control

As for arm and submodule power control, phase-leg power control implies the ability to handle different active power components in each leg without affecting the AC-side. This is what [2] referrers to as horizontal balancing and is adapted to the case of an MMC BESS in [19].

As already mentioned, the DC-component of the circulating current relates the power exchange between a phase-leg and the rest of the converter. In normal MMC operation this is the power exchange to and from the high voltage DC-link. In a split-battery MMC this component is zero, but due to the freedom in the MMC of freely choosing what is called

the common-mode-voltage, v_{cm}, exchange of power between the converter phases can be enabled, without affecting AC- and DC-side.

To understand this energy transfer lets simplify the series connected submodules in each arm into voltage sources containing a fundamental frequency component and a DC-component. As is illustrated in the equivalent circuits in figure 2.6. By dividing the circuit into two, the DC- and AC-components can be analyzed separately, as is done in [20]. Remembering $v_{arm,u}$ and $v_{arm,l}$ in 1.1(b-c) it is obvious that adding an equal voltage, v_{cm}, to both waveforms will not affect the grid voltage, v_g, in 1.1(d). Hence, not inducing any DC-currents. But this *will* induce a DC-current to flow from phase a and split into b and c like the current i_c^{dc} does in the equivalent circuit of figure 2.6. Adding a DC-component to the circulating current, negative in phase a and positive in b and c.

Going back to the arm powers given in (2.8) and (2.9) a negative DC-component of i_c will increase the total phase-leg power, with equal amounts in upper and lower arm. Correspondingly, a positive DC-component of i_c will decrease the phase-leg power. Giving a total power exchange to or from phase k related to i_c of:

$$i_{c,k}^{dc} = \frac{P_k^{transfer}}{V_{dc}} \tag{2.18}$$

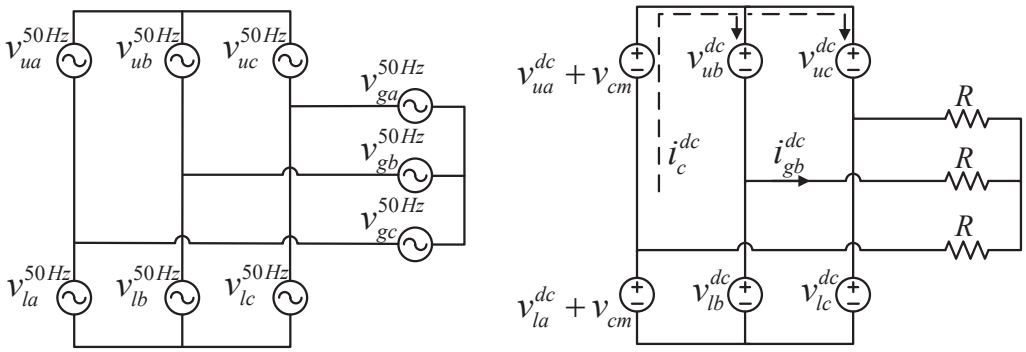

Figure 2.6: MMC circuit split into AC and DC parts

2.3 Balancing with passive interfaces

After establishing the methods for controlling the individual power in submodule, arm and phase, one more detail has do be considered in the case of using passive interfaces. The way the passive interface is defined in this thesis, it can also be described as a direct interface. Meaning that the voltage of the battery has a direct relation to the submodule voltage. As apposed to the active DC-DC interface where these voltages are decoupled, resulting in an indirect interface.
The control system needs to be adapted to this because **1.** batteries with different SOC also have different voltage and **2.** the different power delivered or absorbed when balancing result in a different current going through the batteries, due to the internal battery resistance,

this will also result in different voltage.

At least these two properties counteracts each other. Consider a battery unit with slightly higher SOC then the others. This means that it will have a higher open circuit voltage (OCV). If the battery units are discharging, this unit needs to be loaded with a higher current then the others in order to reach balance again. This will lower the voltage compared to the others. When charging, this unit will need to be charged a bit slower. Also this resulting in a lower voltage. And vice versa for a unit with lower SOC.

Nevertheless, these characteristics results in the need for another control level. With the objective of injecting an extra DC-component in the arm voltage reference as is described in [20], where batteries are directly connected without any filter or active interface to the submodules. This is to counteract the different submodule voltages that could interfere with the balancing control or actually inject DC-current into the AC side.

Chapter 3

The Passive Interface Technique

In most literature the active interface solution for realizing a MMC based BESS is chosen over the passive interface, on the basis of the impediments mentioned in earlier chapters. As a result little or no research has been focused on this passive filter solution. Therefore, in this chapter, a comprehensive analysis will be given on this alternative approach. With the objective to enlighten the challenges of using this type of interface, and possible solutions.

3.1 Submodule and arm dynamics

As already mentioned, the current flowing through the arms in an MMC have large AC-components. This current will flow through the submodules. The MMCs output signal is obviously controlled by the switching of the submodules, and is hence the source of these AC characteristics. Meaning they are inevitable. But to take a closer look at these currents, lets go back to the arm power equations of (2.8) and (2.9) derived in chapter 2.

$$P_{arm,u} = \frac{V_{dc}}{2}\frac{i_g}{2} + \frac{V_{dc}}{2}i_c - v_g\frac{i_g}{2} - v_g i_c \tag{2.8}$$

Arm power for upper arm is here rewritten for reference. And this time, the AC-components are of interest and not the DC-components like in chapter 2. Hence, only one equation is needed. Meaning that the same equation will apply for both upper and lower arm.

As was mentioned in chapter 1, there exists effective control techniques to mitigate the circulating current i_c. Assuming this controller works perfectly,$i_c = 0$, (2.8) reduces to:

$$P_{arm} = \frac{V_{dc}}{2}\frac{i_g}{2} - v_g\frac{i_g}{2} \tag{3.1}$$

And now, by using the trigonometric identity from (2.10), (3.1) can be written as:

$$P_{arm} = \frac{1}{2}\frac{V_{dc}}{2}\hat{i}_g \cos(\omega t + \varphi) - \frac{1}{2}\frac{1}{2}\hat{v}_g\hat{i}_g\Big[\cos(\omega t + \omega t + \varphi) + \cos(\omega t - (\omega t + \varphi))\Big]$$

$$= \frac{1}{2}\frac{V_{dc}}{2}\hat{i}_g \cos(\omega t + \varphi) - \frac{1}{4}\hat{v}_g\hat{i}_g \cos(2\omega t + \varphi) + \frac{1}{4}\hat{v}_g\hat{i}_g \cos(\varphi)) \tag{3.2}$$

(3.2) show the two oscillating terms and the constant term in the power equation. One term oscillating at the fundamental frequency, and the other at the 2nd harmonic frequency.

If a modulation index of unity is assumed, it follows that $\frac{V_{dc}}{2} = \hat{v}_g$. And if the phase angle is assumed to zero, $\varphi = 0$ (no reactive power). (3.2) can be further simplified to:

$$P_{arm} = \frac{1}{4}\hat{i}_g\frac{V_{dc}}{2}\Big[2\cos(\omega t) - \cos(2\omega t) + 1\Big] \tag{3.3}$$

(3.3) clearly show the relation between the magnitudes of the three terms. The fundamental component has a peak amplitude of twice the DC-component, and the 2nd harmonic has the same peak amplitude as the DC-component.

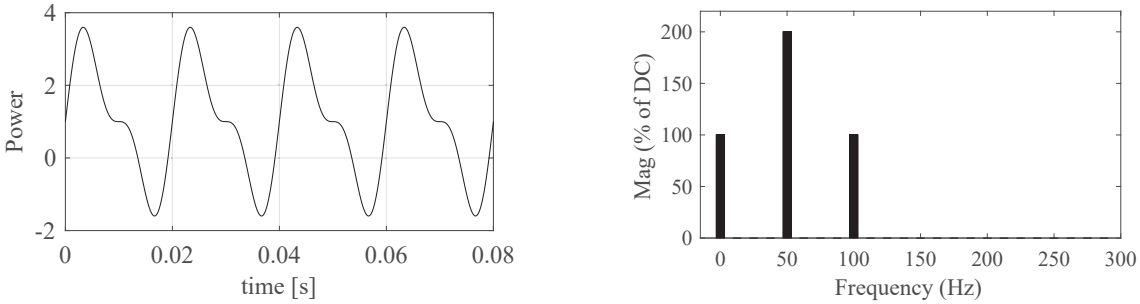

Figure 3.1: P_{arm} from (3.3), waveform and FFT

Figure 3.1 illustrates the waveform given in (3.3). And this waveform is characteristic for MMCs. Its the same waveform as is seen on the voltage of the submodule capacitors in regular MMC operation. This makes sense because its essentially the capacitors that buffers the arm power fluctuations.

But the objective of this analysis was to investigate battery integration in the submodules. And when the batteries are integrated into the submodules, the question of where these arm power fluctuations can be buffered arises. Note that if submodule voltage is assumed constant, the power is proportional with the current. And research on such low order harmonic currents through a battery is not widely available, but it is assumed that it will have an unacceptable effect on battery performance and lifetime. The challenge is therefore to remove or move these power fluctuations out of the battery. In an active interface this is effectively done by the submodule capacitor together with the DC-DC converter. But the impediments of a passive technique is now very clear given the magnitude of the oscillating terms and the fact that they are split into two different low order frequencies.

For a passive filter, a possible solution would be to use a lowpass structure of inductors and capacitors. Tuned to a low enough frequency so that it filters all unwanted oscillating components. Although possible, the large magnitude and low frequency of the signal being filtered, will require very large passive elements. On top of this, inductors in series with the battery will need to carry DC current, inevitably also resulting in more bulky components to avoid saturation. Eventually making this solution not feasible.

In chapter 2, the passive interface in [1] was introduced. Here a resonant filter tuned at the 2nd harmonic frequency was used to interface batteries with the submodules of an CHB. As mentioned the arm power fluctuations in an CHB is only on the 2nd harmonic frequency. So one resonant filter, together with a low pass filter to take higher frequency switching harmonics, is enough to effectively filter the battery current. This technique can be transferred to the case of an MMC, only by adding another resonant filter to attenuate the fundamental component as well. A resonant filter is only capable of filtering one frequency, but requires considerably smaller passive elements compared to a low pass filter at that given frequency, and no inductors in series with the battery taking DC current is needed. This filter, although requiring a considerable amount of large passive elements, could also be a feasible solution. But this alternative is left for later research to explore deeper. Instead a strategy only using one resonant branch is investigated further.

One of the advantages of the MMC is the degree of freedom in the internal dynamics that the circulating current provides. As already mentioned this is a current that flows inside the legs of a 3-phase MMC, not affecting DC-link or AC-side of the converter. The next section will investigate how this current can be used to mitigate the 2nd harmonic arm power component, and together with only one resonant branch in the passive filter, attenuate AC-components in the battery current.

3.2 Injected circulating current and resonant filter

[21] first proposed, but did not explore, the possibility of using the same technique as was presented in [22] to cancel the 2nd harmonic arm power fluctuation with the objective to ease the filtering requirements on a passive filter for interfacing batteries to MMC submodule. This section will go deeper into this method. Firstly, the control technique of circulating current injection, and secondly, interface filter design using resonant filter.

3.2.1 Injecting circulating current to cancel 2nd harmonic

The MMC has many advantages which are being exploited in many different applications. But there is also many challenges on adapting this topology to suit certain applications (which is done in this very thesis). One of these impediments regarding the MMC is to produce a variable frequency output, and especially producing low frequencies. Consider again the arm power equation in (3.1), integrating this equation gives the following arm energy:

$$\begin{aligned} E_{arm} &= \int \Big[\frac{V_{dc}}{2}\frac{\hat{i}_g}{2}\cos(\omega t) - \hat{v}_g\frac{\hat{i}_g}{2}\cos 2\omega t\Big]dt \\ &= \frac{1}{\omega}\frac{V_{dc}}{2}\frac{\hat{i}_g}{2}\sin(\omega t) - \frac{1}{2\omega}\hat{v}_g\frac{\hat{i}_g}{2}\sin(2\omega t) \end{aligned} \tag{3.4}$$

(3.4) show that the peak to peak arm energy fluctuations are inversely proportional to the output frequency. So at low frequencies the energy fluctuations that the capacitors need to buffer will become very large, and approach infinite close to zero frequency. [23] first developed a technique to decouple the arm energy from the output frequency with the intention to adapt the MMC for variable speed drives. And later [22] proposed a similar technique to reduce the peak to peak arm energy fluctuations in the MMC for use in frequency converters for interconnecting the 16.7 Hz rail supply with the 50 Hz grid.

Now the idea is to use the same technique to reduce the filter requirements in the submodule battery interface. Lets go back to the arm power equation in (2.8):

$$P_{arm} = \frac{V_{dc}}{2}\frac{i_g}{2} + \frac{V_{dc}}{2}i_c - v_g\frac{i_g}{2} - v_g i_c \tag{2.8}$$

Instead of using the circulating current controller to mitigate the current, lets inject a current that will cancel some of the arm power fluctuation. Both the power terms in (3.1) have oscillating components. And the 2nd harmonic can be canceled out without affecting AC and DC side of the converter.

Canceling the oscillating component in the third power term in (2.8), $v_g\frac{i_g}{2}$, gives:

$$\Big(-v_g\frac{i_g}{2}\Big)_{AC} + \Big(\frac{V_{dc}}{2}i_c\Big)_{AC} = 0$$

$$i_c = \frac{v_g i_g}{2\frac{V_{dc}}{2}} = \frac{\hat{v}_g\hat{i}_g}{V_{dc}}\frac{1}{(\sqrt{2})^2}\Big[\cos(2\omega t + \varphi) + \cancel{\cos(\varphi)}\Big]$$

$$i_c = \frac{\hat{v}_g \hat{i}_g}{V_{dc}} \frac{1}{2} \cos(2\omega t + \varphi) \tag{3.5}$$

So injecting the circulating current given by (3.5), in phase with the output current, the 2nd harmonic arm power fluctuation will be canceled. Let's try this in (2.8) with ($\varphi = 0$):

$$\begin{aligned} P_{arm} &= \frac{1}{2}\frac{V_{dc}}{2}\hat{i}_g \cos(\omega t) - \cancel{\frac{V_{dc}}{2}\Big[\frac{\hat{v}_g \hat{i}_g}{V_{dc}} \frac{1}{2} \cos(2\omega t)\Big]} - \cancel{\frac{1}{4}\hat{v}_g \hat{i}_g \cos(2\omega t)} + \frac{1}{4}\hat{v}_g \hat{i}_g \\ &\quad - \frac{1}{4\frac{V_{dc}}{2}} \hat{v}_g^2 \hat{i}_g \frac{1}{2}\Big[\cos(2\omega t + \omega t) + \cos(2\omega t - \omega t)\Big] \\ &= \frac{1}{2}\frac{V_{dc}}{2}\hat{i}_g \cos(\omega t) + \frac{1}{4}\hat{v}_g \hat{i}_g - \frac{1}{4\frac{V_{dc}}{2}} \hat{v}_g^2 \hat{i}_g \frac{1}{2}\Big[\cos(3\omega t) + \cos(\omega t)\Big] \end{aligned} \tag{3.6}$$

Again assuming modulation index of unity so that $\frac{V_{dc}}{2} = \hat{v}_g$:

$$= \frac{1}{4}\hat{i}_g \frac{V_{dc}}{2}\Big[1 + \frac{3}{2}\cos(\omega t) - \frac{1}{2}\cos(3\omega t)\Big] \tag{3.7}$$

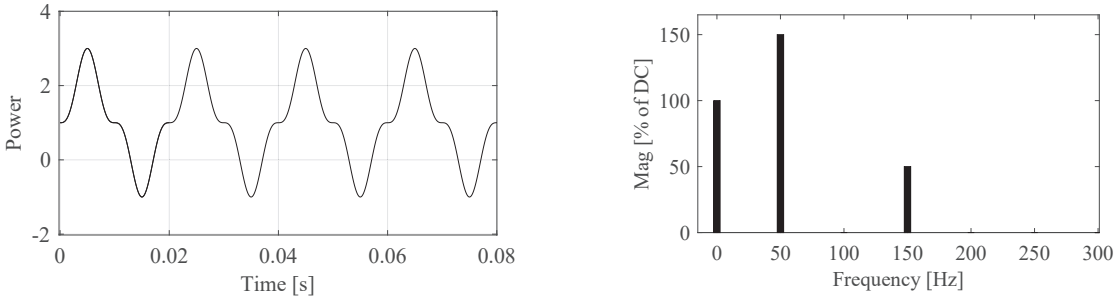

Figure 3.2: P_{arm} from (3.7), waveform and FFT

(3.7) clearly show the effective removal of the 2nd harmonic this technique provides. It also shows that the fundamental component is reduced slightly, but also that a 3rd harmonic component now is present. This is illustrated in figure 3.2.

The power equation in (3.7) provides the characteristics the filter has to attenuate. Remember that since the voltage of the submodules and batteries can be assumed to be constant, the power will be proportional to the current. In the next section a filter will be designed based on the submodule current characteristics found in (3.7).

3.2.2 Filter design

As already discussed, since a large specific frequency is to be filtered in this case, a resonant filter is a very reasonably choice. Meaning a filter that can be tuned to mitigate only one specific frequency. Requiring considerably lower component values compared to other filter arrangements, at that given frequency. But there are also several different types of resonant filters. All using the series connection of inductance and capacitance, but with slightly different setups, giving slightly different characteristics. Some of these variants are given in figure 3.3.

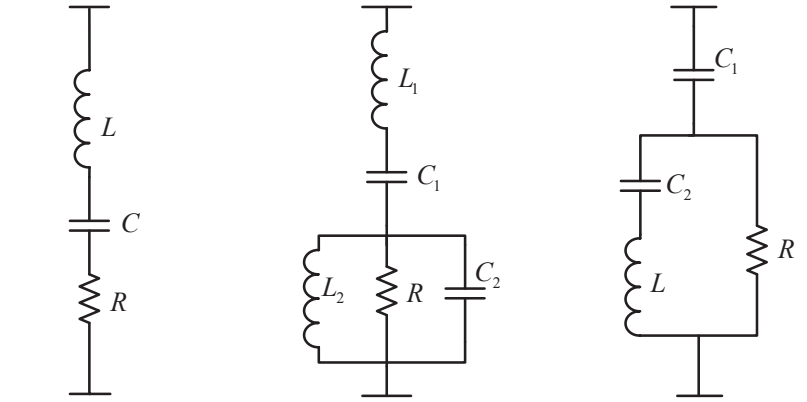

(a) Single-tuned (b) Double-tuned (c) C-type

Figure 3.3: Different resonant filter arrangements

The single-tuned resonant filter given in 3.3(a) is the conventional LC filter arrangement. This arrangement provides the best attenuation of the resonant frequency but as apposed to the C-type filter in 3.3(c) is more sensitive to variations in manufacturing tolerances [24]. Also the double-tuned filter in 3.3(b) [25] can be a good choice, providing two resonant frequencies, that could be tuned to the fundamental and third harmonic.

But since the attenuation performance in this case is of so high importance, the scope of this thesis is limited to the single-tuned filter, which hereafter for simplicity will be referred to as the resonant branch or resonant filter. The use of the other filter arrangements are therefore left for further work to explore.

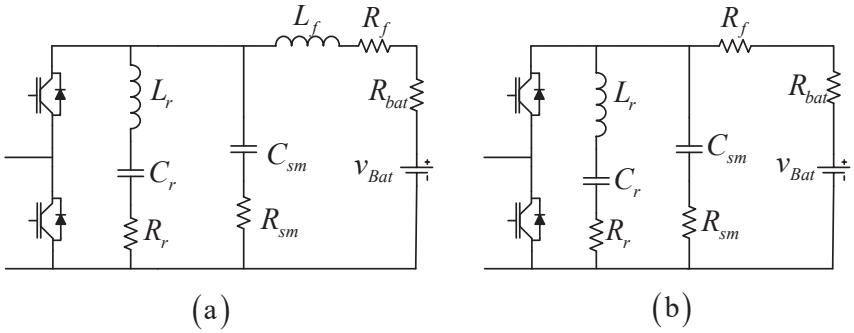

Figure 3.4: Proposed interface filter, (a) with lowpass inductor (b) without lowpass inductor

The complete interface filter, with both the resonant branch and the lowpass branch is pre-

sented in figure 3.4. This is based on the proposed filter in [1], only adapting the resonant filter to the fundamental frequency instead. A case with and without the lowpass inductor will be investigated.

To analyze this filter further, the transfer functions are developed. Starting with the impedance of the three branches of the filter in the s-plane:

$$Z_r = sL_r + \frac{1}{sC_r} + R_r \tag{3.8}$$

$$Z_{sm} = \frac{1}{sC_{sm}} + R_{sm} \tag{3.9}$$

$$Z_{bat(a)} = sL_f + R_f + R_{bat} \tag{3.10}$$

$$Z_{bat(b)} = R_f + R_{bat} \tag{3.11}$$

Setting the expression for Z_r in (3.8) equal to only the resistive term R_r or:

$$sL_r + \frac{1}{sC_r} = 0 \tag{3.12}$$

The frequency that "see" zero impedance from the inductor and capacitor in series can be found easily:

$$\begin{aligned} s^2 L_r C_r &= -1 && (s = j\omega) \\ (j\omega)^2 &= \frac{-1}{L_r C_r} && (j^2 = -1) \\ f_r &= \frac{1}{2\pi\sqrt{L_r C_r}} && (\omega = 2\pi f) \end{aligned} \tag{3.13}$$

Now (3.13) can be used to tune L_r and C_r so that the resonant branch attenuates the fundamental frequency.

Further, using current division, the transfer function from I_{sm} to I_{bat} can be found:

$$TF(s) = \frac{I_{bat}}{I_{sm}} = \frac{Z_r \parallel Z_{sm}}{Z_r \parallel Z_{sm} + Z_{bat}} = \frac{n(s)}{d(s)} \tag{3.14}$$

Where $n(s)$ and $d(s)$ for filter (a) is given in (3.15) on the next page. By setting $L_f = 0$ the transfer function of the filter in 3.4(b) is obtained.

$$
\begin{aligned}
n(s) &= C_{sm}R_{sm}C_rL_rs^3 + \big[C_{sm}R_{sm}C_rR_r + C_rL_r\big]s^2 + \big[C_{sm}R_{sm} + C_rR_r\big]s + 1 \\
d(s) &= C_rC_{sm}L_fL_rs^4 + \\
&\quad \big[C_rC_{sm}L_r(R_{bat}+R_f) + C_rC_{sm}L_fR_r + C_rC_{sm}R_{sm}(L_f+L_r)\big]s^3 \\
&\quad + \big[C_rC_{sm}R_r(R_{bat}+R_f) + C_rC_{sm}R_{sm}(R_{bat}+R_f) + C_rC_{sm}R_rR_{sm} \\
&\quad + C_{sm}L_f + C_r(L_r+L_f)\big]s^2 + \\
&\quad \big[(C_r+C_{sm})(R_{bat}+R_f) + C_rR_r + C_{sm}R_{sm}\big]s + 1
\end{aligned} \tag{3.15}
$$

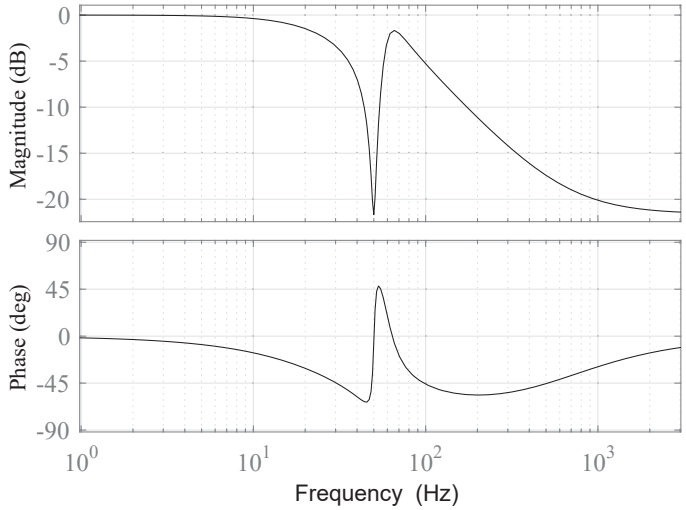

Figure 3.5: Bode plot of (3.14) showing magnitude and phase. Parameter values corresponds to table 3.1

parameter	value
L_r	3.18 mH
C_r	3.18 mF
R_r	0.05 Ω
C_{sm}	5 mF
R_{sm}	0.05 Ω
L_f	0
R_f	0.05 Ω
R_{bat}	0.5 Ω

Table 3.1: Base case parameters

Now, further analysis of this transfer function can be done to tune the filter components and analyze the performance of the filter. The parameter values shown in table 3.1 will be used as a base case, only varying one value at a time to see how this changes the response of the filter. Focusing on revealing the dynamic properties of the filter.

Resonant branch

The bode plot in figure 3.5 show both magnitude and phase. From this plot it is easy to see how the resonant capacitor is dominating the total impedance of the filter until 50 Hz, giving a negative phase shift. After 50 Hz the resonant inductor is dominating, giving a positive phase shift before the lowpass capacitor dominates at higher frequencies. Note also that at exactly 50 Hz the phase is zero, meaning that the only impedance through the resonant filter is the ohmic resistance of R_r. Same goes for very low frequencies or DC and very high frequencies, where the battery resistance R_{bat} and lowpass branch resistance R_f is dominating total impedance respectively.

Its already shown how L_r and C_r is tuned to the specific frequency of 50 Hz, which provides what the value of L_rC_r should be:

$$L_rC_r = \left(\frac{1}{2\pi f_r}\right)^2 \tag{3.16}$$

The bode plot in figure 3.6(a) show impacts of varying the sizes of the capacitor and the inductor, but keeping their product constant. It shows that a large capacitor provides a ”wider” damping area. Giving more margin to the tuning of the resonant frequency i.e lowers sensitivity to manufacturing tolerances. This is very beneficial when dealing with real world components, even though damping only at the specific frequency of 50 Hz is needed.

Figure 3.6(b) show the bode plot of different values of the resonant resistance R_r. In many cases this resistance is chosen to $R_r = \sqrt{2}\sqrt{\frac{L_r}{C_r}}$ to optimize the performance of the filter. In this case this will result in a fairly large resistance and as the bode plot show, higher resistance reduces the damping at the resonant frequency but adds more damping after. In this case a good damping of the resonant filter is crucial and not the frequencies around. So a low R_r is preferred. This makes sense since a 50 Hz current only ”see” the ohmic resistance of the resonant branch and the battery branch. The ratio between these resistances will decide how the current is devided into each branch. Minimizing ESR is therefore crucial in the resonant branch to achieve optimal damping performance.

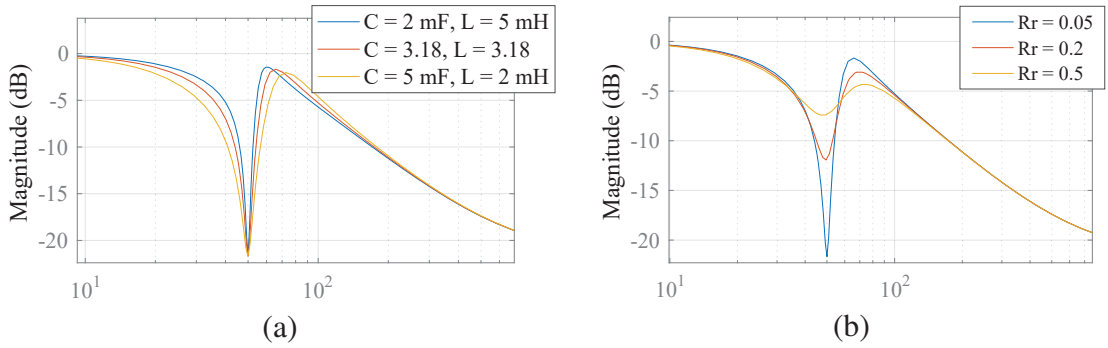

Figure 3.6: Bode plot with [Hz] on x-axis, (a) varying C_r and (b) varying R_r in resonant branch

Lowpass

The question at hand regarding the lowass filter is sizing of the capacitor C_{sm} and whether or not the inductor L_f is beneficial in a feasible size.

Figure 3.7(a) show the bode plot of filter (a) with varying size on the inductor. For the two lowest values the inductor makes very little difference, first closer to 1 mH there are noticeable changes. At this size the inductor enhances the performance of the filter. Providing more damping to the 150 Hz component as well as the switching harmonics.

The inductors required here need to carry DC current, typically meaning air-core inductors, these are more bulky at higher inductance values, which could turn out problematic when realizing this filter.

Also a high inductor value causes a resonant top, shortly after the fundamental frequency. This could also be problematic, especially if the control technique fails to completely mitigate the 2nd harmonic. For these reasons, the case without the inductor is also considered.

And figure 3.7(b) show bode plots of filter (b) with varying size on the lowpass capacitor C_{sm}. It shows that a considerable value is needed to attenuate the 150 Hz component, but that this filter with a large enough capacitor can provide adequate performance without the inductor.

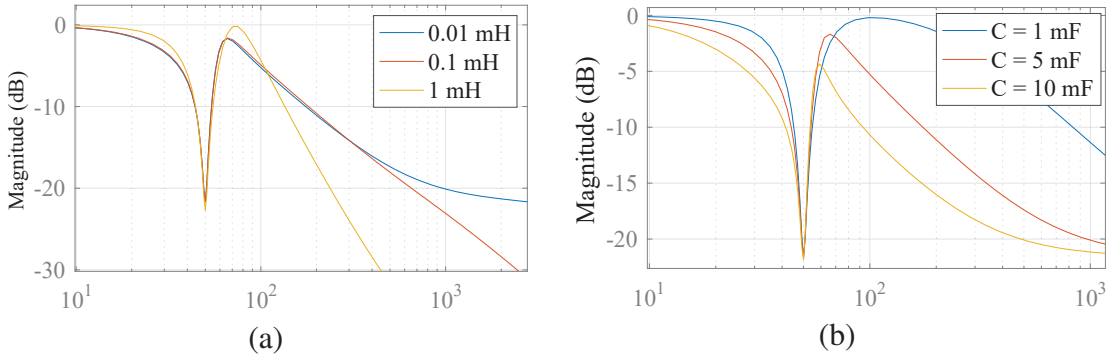

Figure 3.7: Bode plot with [Hz] on x-axis, (a) varying lowpass inductance L_f and (b) varying lowpass capacitor C_{sm}

Battery resistance

There is one last parameter that has a large effect on the characteristics of the filter. That is the battery resistance. It has already been mentioned regarding the resonant branch, that its damping performance relates to the ratio of the battery resistance (or $R_{bat} + R_f$) and resonant ESR, R_r. Unfortunately the battery internal resistance is not constant, but varies with current drawn through the battery (figure 5.2(b)), temperature, SOC and age. It also behaves slightly different when it is charging from when it is discharging. All these factors will again have an effect on the filter performance and needs to be taken into account in the filter design. The bode plot in figure 5.2(a) show that for higher resistance, the filter provides more damping. For lower values, the filter provides less damping at all frequencies.

Battery cells are series connected to reach a certain system voltage. This increases the resistance since the resistance of each cell is series connected. But to increase the capacity at that voltage, cells are paralleled. This decreases the total battery resistance. Meaning that especially for BESS with larger capacities the importance of a low resonant branch ESR is even more crucial for the performance of the filter.

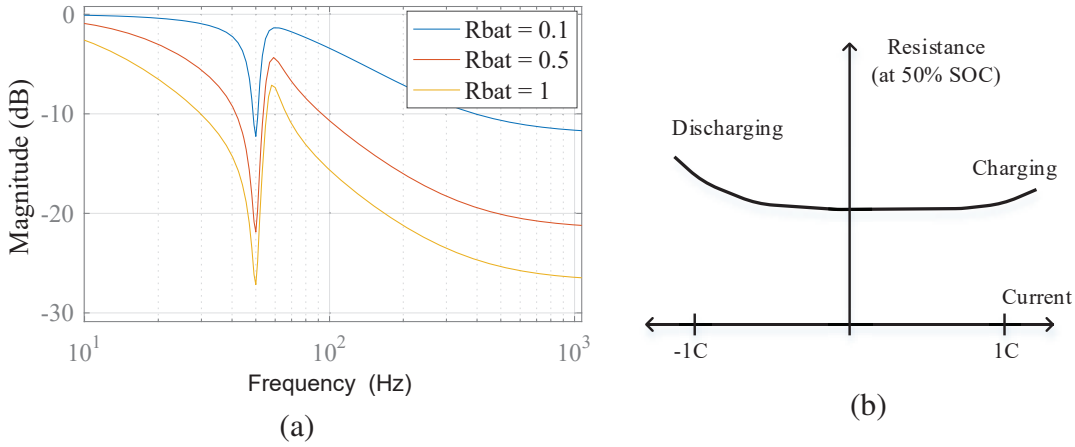

Figure 3.8: (a) Bode plot with varying battery resistance and (b) typical battery resistance at different charge and discharge currents

3.3 Loss calculation

All power converters will inevitably introduce some losses in the power flow. And in the case of a BESS, power is dissipated both in the converter and in the batteries them self. To provide a full picture of the power losses, extensive research on every part of the power flow is needed. That is outside the scope of this thesis, which will be limited to a short analytic calculation on the losses specific to the filter strategy presented throughout this chapter. Meaning **1.** the losses introduced inside the converter due to the injected circulating current, and **2.** the losses in the passive interface filter.

These losses would not be present if an active DC-DC converter was chosen to interface the batteries to the submodules. Which is the main case to compare with.

Possible losses in the batteries because the filter is unable to completely filter all low order frequencies are left for further work.

3.3.1 Injected circulating current

In regular MMC operation or in the case of using DC-DC converters as battery interfaces, the circulating current would be suppressed to increase efficiency. So injecting a circulating current will obviously introduce an extra source of power loss. Increasing the current that flows through the switches and diodes of the submodules and also through the ESR of the arm inductor.

Calculating the losses from the IGBTs or MOSFETs and the anti-parallel diodes is an intricate process. Taking into account conduction losses, turn-on and turn-off losses, reverse recovery losses and so on. But many of these losses are close to proportional to the square of the RMS current that flows through them. And by doing this simplification, calculating the increased RMS value of the arm current will give an indication of how much the internal converter losses increases with the injected circulating current.
First, without any circulating current:

$$i_{arm}^{rms} = \sqrt{\frac{1}{T}\int_{t}^{t+T}\left(\frac{\hat{i}_g}{2}\cos\omega t\right)^2 dt} = \frac{1}{2\sqrt{2}}\hat{i}_g = 0.354\,\hat{i}_g \tag{3.17}$$

Then, injecting circulating current with peak amplitude of $\frac{\hat{v}_g\hat{i}_g}{2V_{dc}}$ which can be simplified to $\frac{\hat{i}_g}{4}$ with modulation ratio of 1 so that $\frac{V_{dc}}{2} = \hat{v}_g$, gives:

$$i_{arm,inj}^{rms} = \sqrt{\frac{1}{T}\int_{t}^{t+T}\left(\frac{\hat{i}_g}{2}\cos\omega t + \frac{\hat{i}_g}{4}\cos 2\omega t\right)^2 dt} \tag{3.18}$$

Doing the integration's in (3.18) results in:

$$i_{arm,inj}^{rms} = \sqrt{\frac{1}{2}\left(\frac{\hat{i}_g}{2}\right)^2 + \frac{1}{2}\left(\frac{\hat{i}_g}{4}\right)^2} = \sqrt{\frac{5}{32}}\,\hat{i}_g = 0.395\,\hat{i}_g \tag{3.19}$$

This corresponds to an increase of $\frac{0.395}{0.354} = 11.6\,\%$, which will increase RI^2 losses with $24.5\,\%$.

This is a very rough estimate of increased internal losses but gives an idea of what they could be. And even though 24.5 % sounds like much, remember that the MMC in general have very low internal losses. Which might mean a total decrease of efficiency in the range of a few percent. But further research on this area is needed to give a more accurate and reliable estimate.

3.3.2 Filter

The loss estimation in the filter is here limited to the RI^2 power dissipation in the resonant branch and the lowpass branch. The amplitude of these branch currents in relation to the DC current is known if it is assumed that the entire fundamental and 3rd harmonic components are filtered through them. Their RMS currents can then easily be found.

$$i_{fnd} = \frac{1}{\sqrt{2}}\frac{3}{2}i_{DC} \quad \text{and} \quad i_{3rd} = \frac{1}{\sqrt{2}}\frac{1}{2}i_{DC} \tag{3.20}$$

Again the power dissipation is to be calculated from $P = RI^2$, but this requires that the resistance in each of the branches are known. This depends on the components used. But as was shown in this chapter, optimizing the filter performance means minimizing the ESR in the branches. So a low resistance can be expected, and is even necessary for the filter to work properly.

Lets do an example then, using $R_r = R_f = 0.5\,\Omega$ and $i_{DC} = 1A$, this will give:

$$P_{filter} = 0.5\left(\frac{3}{2\sqrt{2}} + \frac{1}{2\sqrt{2}}\right)^2 = 1\,W \tag{3.21}$$

At a battery unit voltage of 100V, hence a battery power of 100W, this will result in total filter losses of 1 %.

Again, these are very simple and rough calculations, neglecting core losses and skin effect in the inductors among others. And further research should be devoted to this area to provide a clearer picture, which could be further compared to the alternative solutions using DC-DC converters or other passive filter configurations.

Chapter 4

Simulation

Seeking verification of the proposed technique a simulation model has been developed and analyzed.

4.1 Simulation model

The model used in the simulations are developed in Matlab/Simulink using the Simscape Power System library. This makes it possible to build a very accurate model down to each component in the system. As a result the simulation runtime is long even for short simulation times. But since the objective is to analyze behaviour inside the converter and inside the submodules, this accuracy is needed. And since long simulation times is *not* needed, the model can still provide useful data relatively fast.

The model is running with a pure ohmic 3-phase load. Uses phase shifted PWM modulation. The AC-side current and voltage is running open loop (no controller) but the circulating current is controlled. Enabling both suppression or injection of circulating current at the 2nd harmonic frequency. In appendix A, a circuit overview of the model is given.

Table 4.1 provides the key parameters for both the MMC and the interface filter.

MMC parameters		**Filter parameters**	
Number of submodules per arm	$N_{sm} = 4$	L_r	10.13 mH
Arm inductance	$L_{arm} = 1$ mH	C_r	1 mF
Open circuit battery voltage	$V_{oc} = 300$ V	R_r	0.1 Ω
Load Resistance	100 Ω	C_{sm}	2 mF
Modulation index	m = 1	R_{sm}	0.01 Ω
Carrier frequency (PS PWM)	$f_{PWM} = 800$ Hz	L_f	0
Fundamental frequency	$f_{ac} = 50$ Hz	R_{bat}	2 Ω

Table 4.1: MMC and Filter parameters in simulation model

4.2 Results

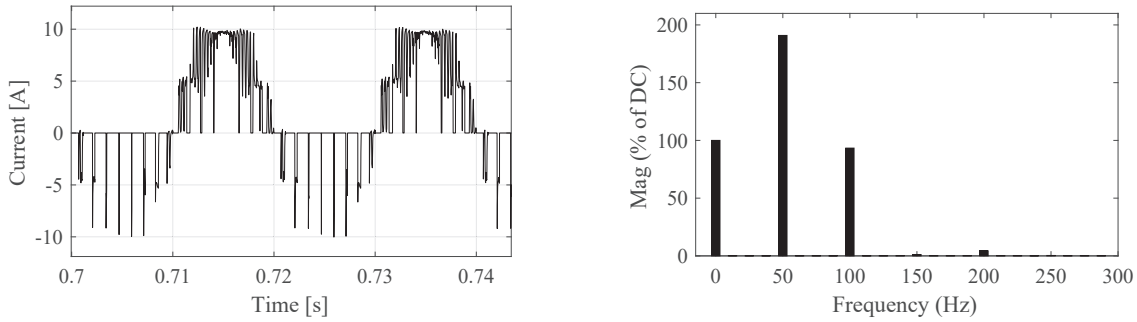

Figure 4.1: Submodule current, i_{sm}, with suppressed circulating current, $i_c = 0$, waveform and FFT

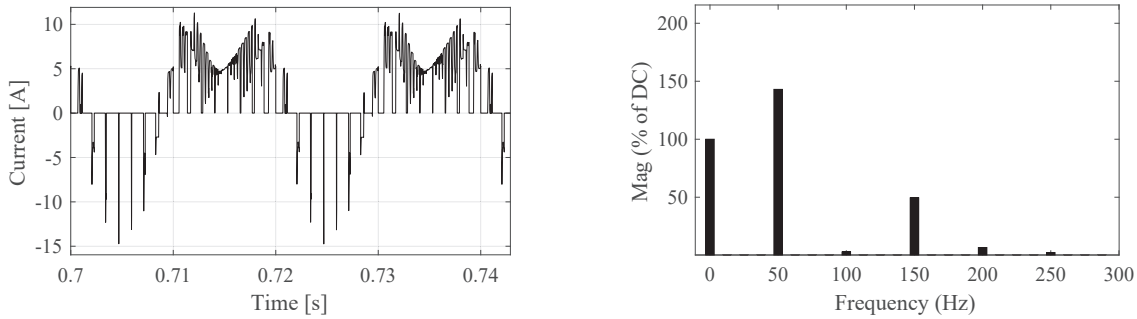

Figure 4.2: submodule current, i_{sm}, with injected circulating current, $\hat{i}_c = \frac{\hat{v}_{ac}\hat{i}_{ac}}{2V_{dc}}$, waveform and FFT

Figure 4.1 show the current flowing through the submodules of the converter, when the circulating current is completely suppressed. Without any balancing currents and already perfectly balanced batteries, this current is identical in all submodules. The FFT is also given in the figure, and it confirms what was calculated in chapter 3. Since the voltage ripple of the submodules are small compared to the DC component, the arm power fluctuation shown in figure 3.1 is similar to the submodule current fluctuations. The simulation show that the fundamental 50 Hz component has a magnitude of 191 % and the 100 Hz is 93.3 % relative to the DC component of 2.57 A.

In figure 4.2 the same current is shown. Only now the controller injects a circulating current that lowers the power fluctuation, which was derived in chapter 3. Again the FFT reveals the same characteristics as was calculated and shown in figure 3.2. The 50 Hz component is lowered to 143.0 %, the 100 Hz is down to 2.79 % but a 150 Hz has also appeared with 49.5 % relative to the DC component still at 2.57 A.

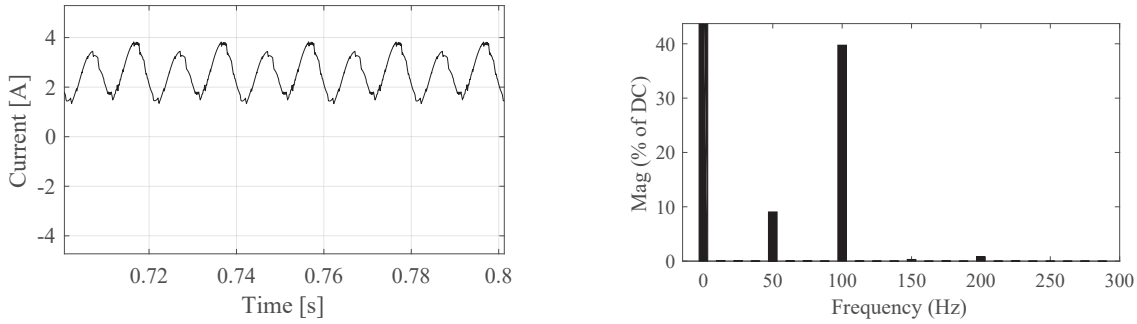

Figure 4.3: Battery current, i_{bat}, with suppressed circulating current, $i_c = 0$, waveform and FFT

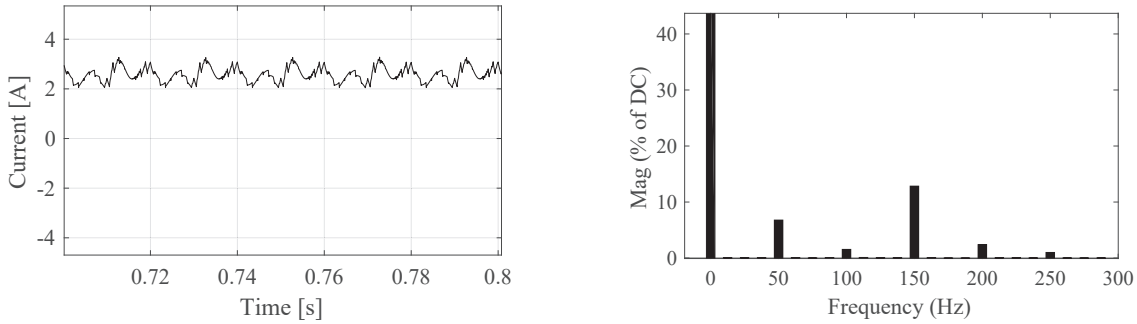

Figure 4.4: Battery current, i_{bat}, with injected circulating current, $\hat{i}_c = \frac{\hat{v}_{ac}\hat{i}_{ac}}{2V_{dc}}$, waveform and FFT

Figure 4.3 and 4.4 show the battery currents in the model. Again split into the case of suppressed circulating current and the case of injected circulating current. The FFT in 4.3 show that the resonant branch is attenuating the 50 Hz component, which is reduced to 9.05 %. The low pass capacitor is also providing some damping of the 100 Hz component which is now down to 39.7 %. This gives a THD of 40.9 %

Figure 4.4 show that with the injected circulating current also the 100 Hz is attenuated. Resulting in a 6.78 % 50 Hz and a 1.55 % 100 Hz component. But again a new 150 Hz component is introduced. Now with a magnitude of 12.8 %. Resulting in a THD of 15.4 %. Both cases with a DC component of 2.57 A.

To get even better damping by the filter, R_r needs to be lowered for better 50 Hz mitigation, and larger C_{sm} or alternatively a lowpass inductor needs to be implemented to mitigate the 150 Hz component.

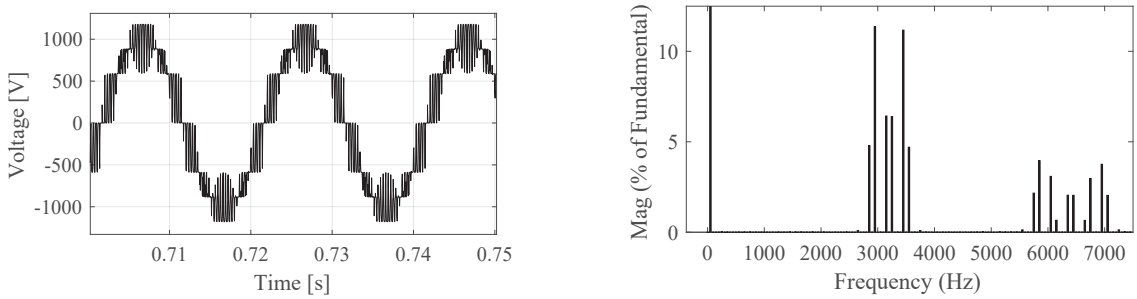

Figure 4.5: Line-to-line voltage output and its FFT

Figure 4.5 finally show that the AC side is unaffected by the injected circulating current. Showing typical FFT results, with harmonic bands located around $N * f_{PWM} = 3200Hz$, according to the PSPWM modulation technique. THD of 21.91 % as apposed to 21.95 % with completely suppressed circulating current.

Chapter 5

Lab

Throughout the work of this thesis an MMC prototype has been designed and is being built. This has mainly been done by phd Anirudh Budnar Acharya, but also me and my fellow MMC master students, David Krogager Dolva and Gard Lyng Rødal, have participated in design and soldering. Unfortunately, time aspect on such projects are difficult to predict and it is now clear that the prototype will not be ready for testing until next semester. Therefore, to provide some lab results, a resonant filter have been built, since this is a main component in the proposed technique. Due to very limited time for testing, the filter was only analyzed with a frequency sweep using a function generator. Although a very simple test, it provided some results and gave some insight on realizing a design with real-world components.

5.1 Setup

The filter was built using film capacitors and radially leaded inductors. As the circuit of figure 5.1 show, two capacitors are paralleled to the combined value of 200μF and three inductors are series connected to the combined value of 50 mH. This should result in a resonant frequency of:

$$f_r = \frac{1}{2\pi\sqrt{L_r C_r}} = \frac{1}{2\pi\sqrt{200 * 50 * 10^{-9}}} = 50.3Hz \tag{5.1}$$

Further, a resistance of 10 Ω is connected in parallel with the filter.

Now the function generator can be used to produce a sinusoidal voltage over the filter. This is set to its maximum peak-to-peak value. Only there is a maximum current this generator can deliver. And this maximum current is already reached with a 10 Ω resistor connected to it. Therefore, essentially this generator works as a current source, delivering a constant current. Hence, simply using ohm's law, it can be derived that the total impedance of the parallel connected filter and 10 Ω resistor is proportional to the voltage over the filter.

Sweeping over a range of frequencies, the frequency response of the filter impedance can be found.

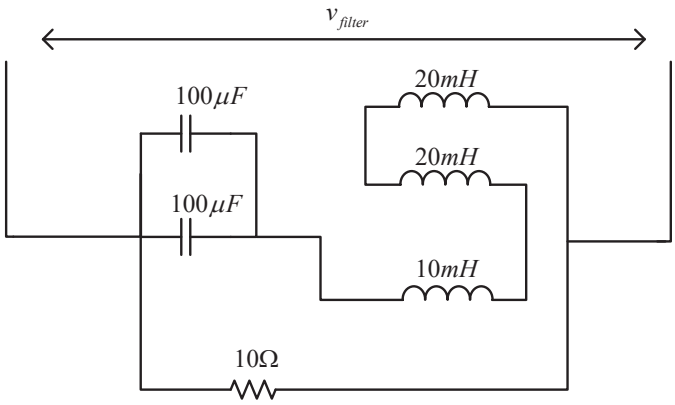

Figure 5.1: Lab filter circuit

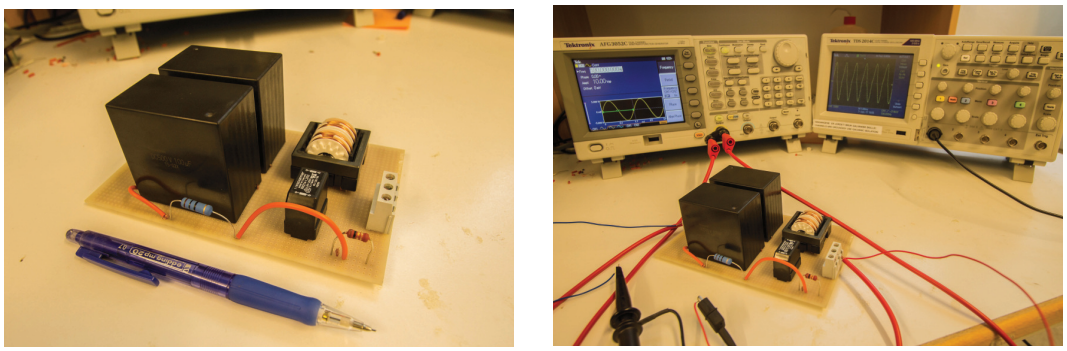

(a) (b)

Figure 5.2: (a) Close-up of filter (b) test setup, function generator (left) and oscilloscope (right)

5.2 Results

The complete results of the frequency sweep is shown in figure 5.3(a), where the response is plotted with voltage on y-axis in normal scale and frequency on x-axis in logarithmic scale. (b-d) also show how the voltage amplitude is larger both at lower and higher frequencies than the resonant frequency. Meaning that the impedance of the resonant branch must be way lower at the resonant frequency. Which is exactly what the filter is designed for.

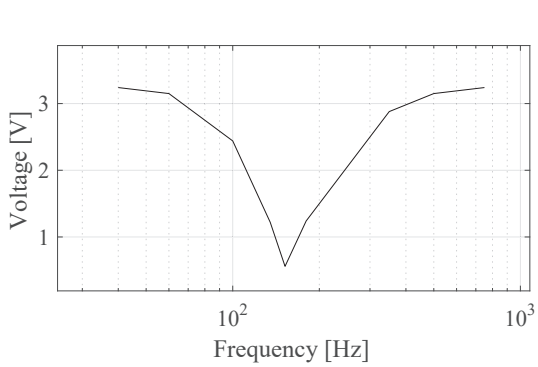

(a)

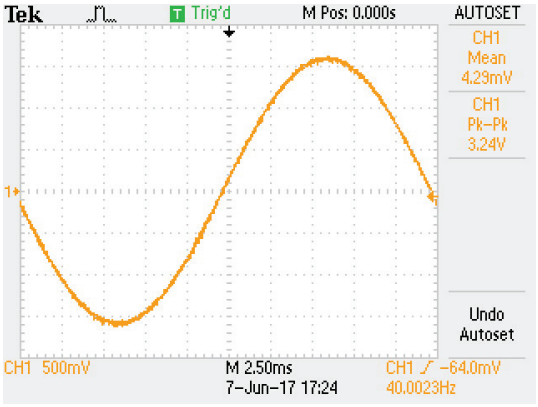

(b) 40 Hz

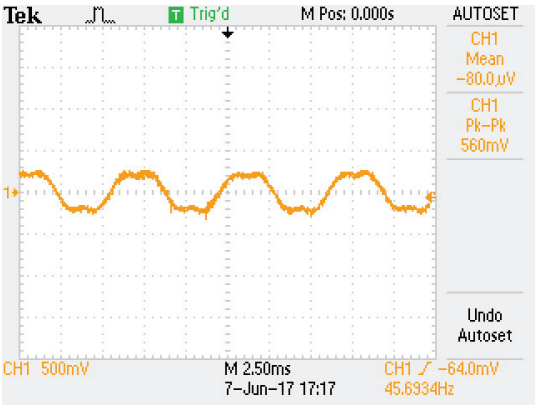

(c) 152 Hz

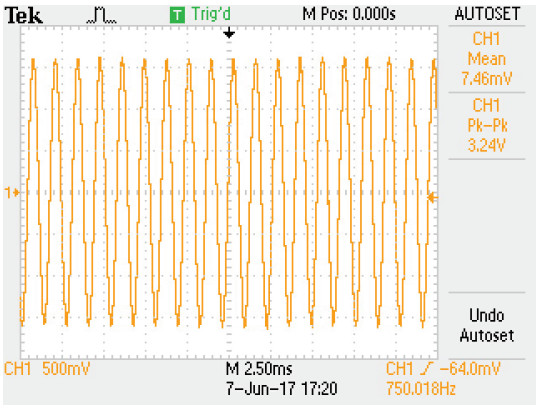

(d) 750 Hz

Figure 5.3: (a) Bode plot with varying battery resistance and (b) typical battery resistance at different charge and discharge currents

A closer look at the results reveal that the impedance is reduced to $\frac{0.56V}{3.24V} = 17\%$ at the resonant frequency. Meaning that the total ESR of the resonant branch should be around 17 % of the paralleled resistance of 10 Ω. Which further means that 83 % of an oscillating component at the resonant frequency would be diverted through the resonant branch rather then the battery. This should be regarded as a minimum.

But usually the battery resistance is considerably less than 10 Ω. This means that the ESR of the resonant branch needs to be lowered even more. Off course this resistance can be somewhat lowered with better soldering, but most of that resistance is due to the inductors. Which in this filter have a combined ESR of as much as 1.2 Ω, according to ohmmeter measurements. To lower this, either more bulky inductors with lower ESR needs to be used or, even better, lower the total inductance. This requires a higher capacitance to keep the resonant frequency. But that will also lower ESR in the capacitors, since they are paralleled to increase capacitance. So increasing capacitance and lowering inductance will lower the ESR in all components. win-win.

But on the other hand, the problem with this solution is the size of those capacitors. Especially film capacitors would be extremely bulky. Therefore, electrolytic capacitors

should be considered instead. These can comprise way higher capacitive storage in the same size. Although, due to safety concerns of using electrolytic capacitors, more time is required in the design of such a filter, but nevertheless, results of this experiment indicate that this is necessary to realize a filter in feasible size and with low enough ESR to perform well.

Finally, the response of this filter is as expected, except that the resonant frequency is way higher than what was estimated (152 Hz). Unfortunately real-world components do not necessarily have the precise rated value found in the data sheet, and on top of that, the mutual inductance of the inductors can have a large effect on the total inductance. Especially in this case where the two 20 mH inducotors are built into the same component. Due to limited time on this experiment, tweaking with the component values to reach the right resonant frequency is postponed to future work. As is testing this filter with the signal that it is supposed to filter, namely a fundamental component on top of a DC component. In lab there are diode rectifiers available. These produce a very similar output as the submodules in an MMC. So the next step to test this filter further, would be to actually tune it to 50 Hz and then test its performance with the diode rectifier output, preferably also building a filter based on electrolytic capacitors.

Conclusion and Further work

This thesis has investigated the alternative solution of using passive filters as interfaces between the batteries and the submodules of the MMC. It has advocated for the benefits of using the MMC split storage arrangement in BESS, and also shown the challenges of connecting the battery units to such a system. Large AC components of fundamental and 2nd harmonic frequency needs to be attenuated by control system or filter, if batteries are to operate optimally throughout their lifetime.

The proposed technique is two-legged **1.** inject a circulating current that attenuates the 2nd harmonic. This technique has theoretically been proven effective and then verified in simulations. The results also corresponds to the given references. This thesis therefore indicate that this technique can be applied and solve its intended task.

2. A filter is placed between battery and submodule to attenuate fundamental component and other frequencies. A combination of a resonant branch and a lowpass branch is proposed and investigated. Theoretically it has been shown that with the right component values available, the filter can be tuned to reduce the targeted AC components to a considerably lower level. Simulations back this up. Lab experiment also indicate that the resonant filter works as intended, but that achieving low enough ESR could be a challenge. Requiring low inductance and high capacitance, hence electrolytic capacitors will be needed to realize the filter in a feasible size.

As apposed to the active DC-DC converter interface, which also provides these benefits, the passive filter is more reliable and provides a less complex structure. It is therefore concluded that the passive technique *could* be an attractive alternative, especially for applications where reliability is of high concern.

However, the choice of direct interfaces needs to be addressed for battery balancing control. Inevitably leading to a more complex design of the balancing control system. But it has been left for further work to completely verify this technique with the proposed filter.

Also, the loss estimations of the proposed technique presented in this thesis, are very simple. Leaving a more comprehensive analysis as further work. Which would have to compare to relevant alternatives.

And third, other passive filter arrangements, such as C-type filter [24] and double tuned filter [25], should be explored as alternatives to the simple resonant filter investigated in this thesis.

Finally, this thesis can only conclude that the results are indicating that the proposed technique works as intended. And that it *could* turn out to be an attractive solution, at least in certain applications. But further work on the areas mentioned here and finally hardware tests on a prototype should be carried out to completely verify and provide an even clearer picture on the pros and cons of this solution.

Bibliography

[1] M. Vasiladiotis, A. Rufer, and A. Bguin, "Modular converter architecture for medium voltage ultra fast ev charging stations: Global system considerations," in *Electric Vehicle Conference (IEVC)*, Greenville, USA, 2012.

[2] P. Mnch *et al.*, "Integrated current control, energy control and energy balancing of modular multilevel converters," in *Annual Conference on IEEE Industrial Electronics Society (IECON)*, Glendale, USA, 2010.

[3] L. X. Q. Tu, Z. Xu, "Reduced switching-frequency modulation and circulating current suppression for modular multilevel converters," *Transactions on Power Delivery*, vol. 26, no. 3, pp. 2009–2017, 2011.

[4] A. Lesnicar and R. Marquardt, "An innovative modular multilevel converter topology suitable for a wide power range," in *IEEE Power Tech Conference Proceedings*, Bologna, Italy, 2003.

[5] R. Baker and L. Bannister, "Electric power converter," patent US 3 867 643, 1975.

[6] M. Hiller *et al.*, "A new highly modular medium voltage converter topology for industrial applications," in *Proc. of the 13th European Conference on Power Electronics and Applications (EPE)*, Barcelona, Spain, 2009.

[7] E. Solas *et al.*, "Modular multilevel converter with different submodule concepts-part 1: Capacitor voltage balancing method," *IEEE Transactions on Industrial Electronics*, pp. 4525–4535, 2013.

[8] G. P. Adam *et al.*, "Modular multilevel inverter: Pulse width modulation and capacitor balancing technique," *IET Power Electronics*, vol. 3, pp. 702–715, 2010.

[9] B. Li *et al.*, "Analysis of the phase-shifted carrier modulation for modular multilevel converters," in *IEEE 15th Workshop on Control and Modeling for Power Electronics (COMPEL)*, Santander, Spain, 2014.

[10] X. Liu, A. Lindeman, and H. Amiri, "Theoretical and experimental comparison of different control strategies for modular multilevel converters," *International Journal of Renewable Energy Research*, vol. 6, no. 3, 2016.

[11] A. Hassanpoor *et al.*, "Harmonic and experimental comparison of different control strategies for modular multilevel converters," in *38th Annual Conference on IEEE Industrial Electronics Society (IECON)*, Montreal, Canada, 2012.

[12] Y. Deng *et al.*, "A fast and generalized space vector modulation scheme for multilevel inverters," *IEEE Transactions on Power Electronics*, vol. 29, pp. 5204–5217, 2014.

[13] Y. Deng and R. Harley, "Space-vector versus nearest-level pulse width modulation for multilevel converters," *IEEE Transaction on Power Electronics*, vol. 30, pp. 2962–2974, 2015.

[14] G. Konstantinou, M. Ciobotaru, and V. Agelidis, "Selective harmonic elimination pulse-width modulation of modular multilevel converters," *IET Power Electronics*, vol. 6, pp. 96–107, 2013.

[15] P. S. Prasanna *et al.*, "A comparative analysis of circulating current controllers for modular multilevel converters," in *Annual IEEE India Conference (INDICON)*, New Delhi, India, 2015.

[16] W. E. Council, "World energy resources full report 2016," *Used by permission of the World Energy Council*, 2016.

[17] M. Schroeder *et al.*, "Integration of batteries into a modular multilevel converter," in *15th European Conference on Power Electronics and Application (ICRERA)*, Lille, France, 2013.

[18] A. Lachichi, "Modular multilevel converters with integrated batteries energy storage," in *International Conference on Renewable Energy Research and Application (ICRERA)*, Milwaukee, USA, 2014.

[19] M. Vasiladiotis and A. Rufer, "Analysis and control of modular multilevel converters with integrated battery energy storage," *IEEE Transactions on Power Electronics*, vol. 30, no. 1, pp. 163–175, 2015.

[20] F. Gao *et al.*, "State-of-charge balancing control strategy of battery energy storage system based on modular multilevel converter," in *IEEE Energy Conversion Congress and Exposition (ECCE)*, Pittsburgh, USA, 2014.

[21] M. Vasiladiotis, "Modular multilevel converters with integrated split battery energy storage," Ph.D. dissertation, École Polytechnique Fédérale de Lausanne (EPFL), Lausanne, Switzerland, 2014.

[22] A. Korn, M. Winkelnkemper, and P. Steimer, "A modular direct converter for transformerless rail interties," *2010 IEEE International Symposium on Industrial Electronics*, pp. 562–567, July 2010.

[23] ——, “Low output frequency operation of the modular multi-level converter,” in *IEEE Energy Conversion Congress and Exposition*, Atlanta, USA, 2010.

[24] R. Dwyer, H. V. Nguyen, and S. G. Ashmore, “C filters for wide-bandwith harmonic attenuation with low losses,” in *IEEE Power Engineering Society Winter Meeting. Conference Proceedings (Cat. No.00CH37077)*, Singapore, 2000.

[25] M. A. Zamani and M. Mohseni, “Damped-type double tuned filters design for hvdc systems,” in *9th International Conference on Electrical Power Quality and Utilisation*, Barcelona, Spain, 2007.

Appendix

A Matlab/Simulink model

The most important parameters are already given in chapter 4. Adding to that, here is the circuit overview of the most important layers of the model.

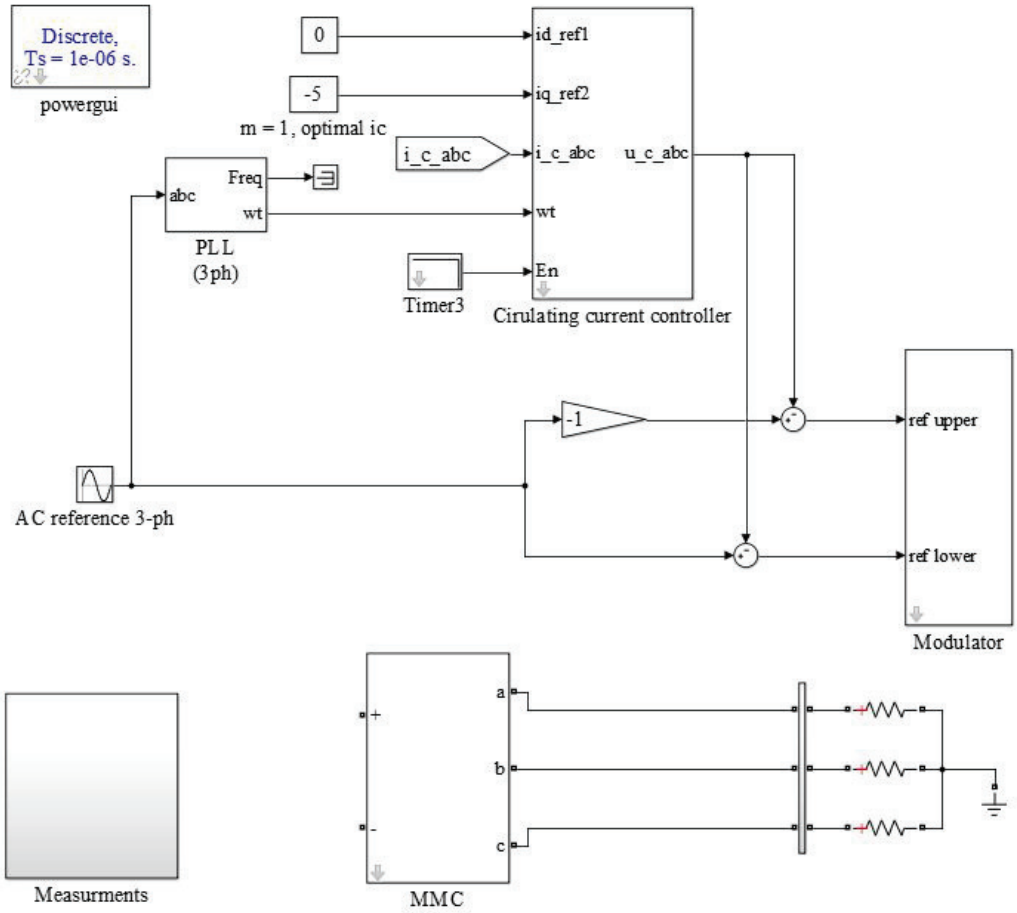

Figure A.1: Top level, overview

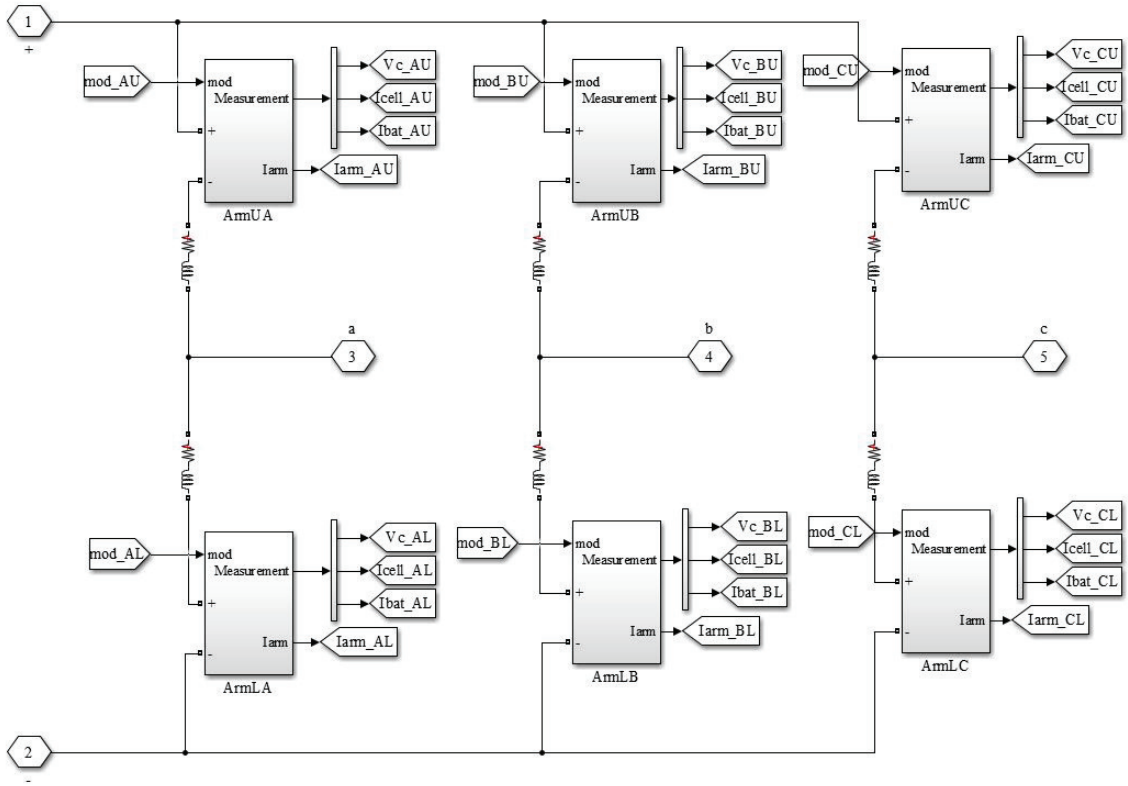

Figure A.2: The MMC circuit, showing the three phase-legs

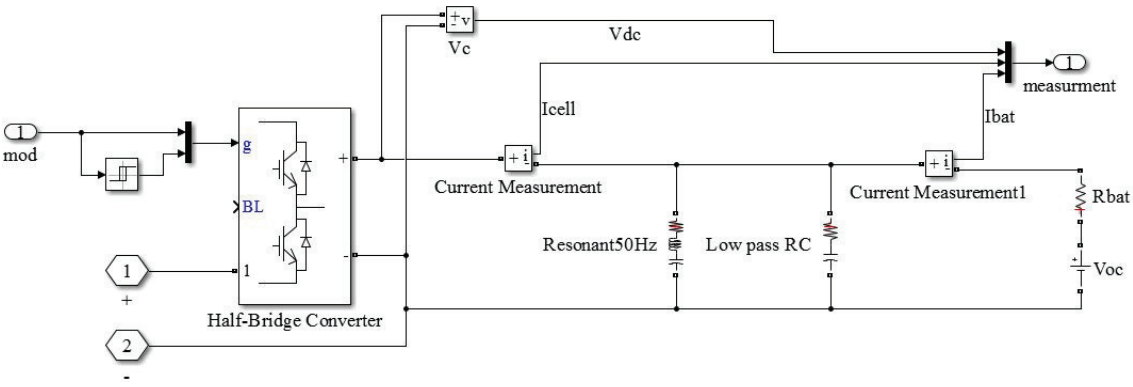

Figure A.3: Submodule, interface filter and battery

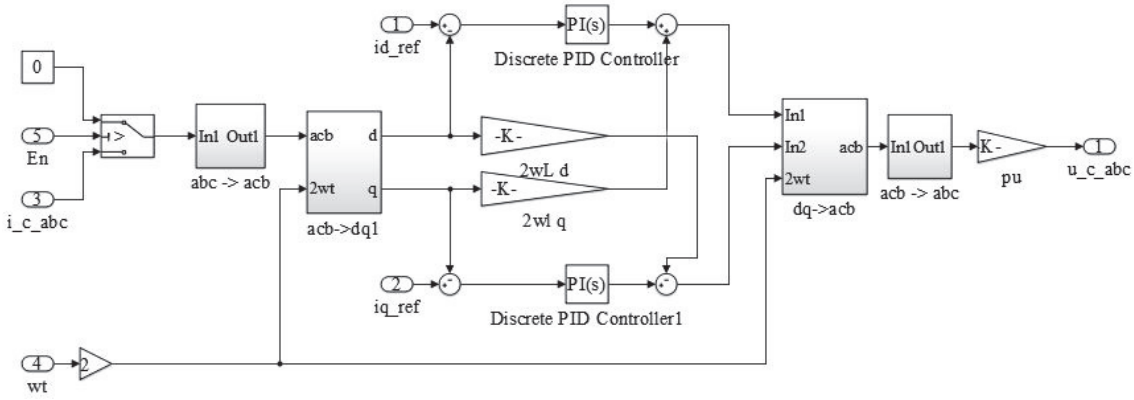

Figure A.4: Circulating current controller based on [3]

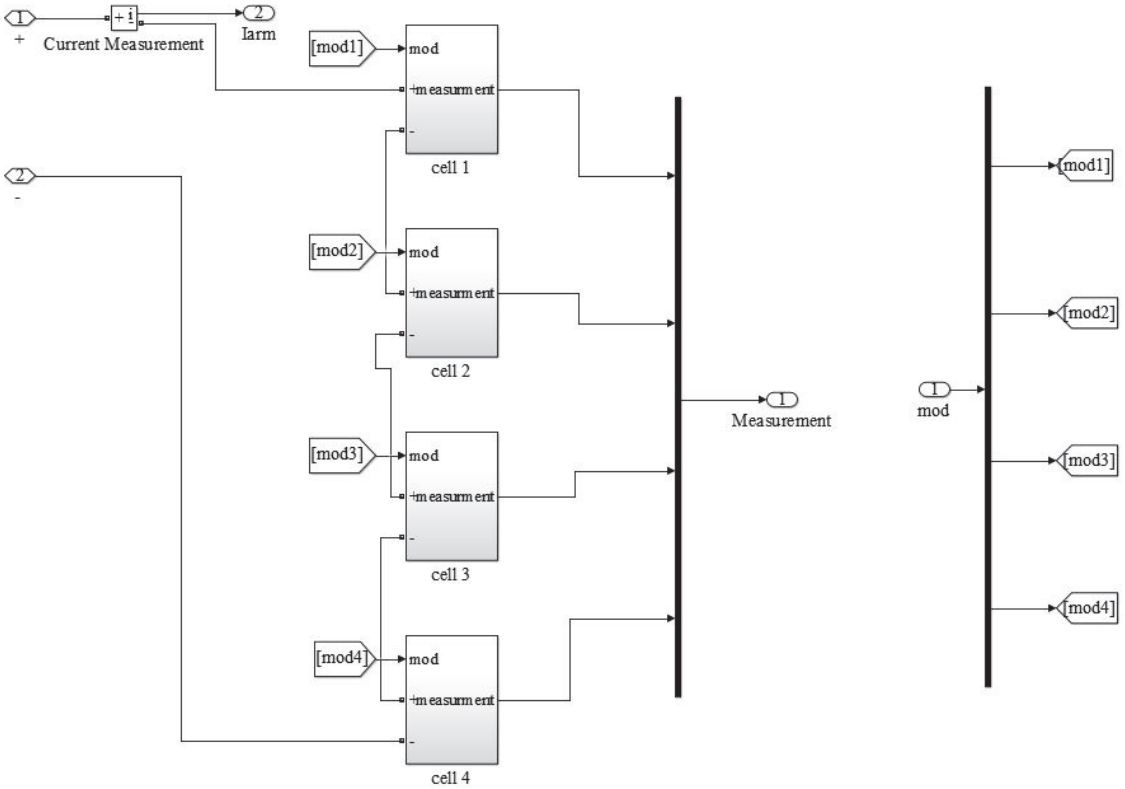

Figure A.5: Arm configuration